การก่อตัวของโครงสร้างนาโนอินเดียมอาร์เซไนด์ที่บางกว่าความหนาวิกฤตบนแผ่นฐานลายตาราง อินเดียมแกลเลียมอาร์เซไนด์โดยการแอนนีลแบบอินซิทู

นายวิน เอี้ยววงษ์เจริญ

บทคัดย่อและแฟ้มข้อมูลฉบับเต็มของวิทยานิพนธ์ตั้งแต่ปีการศึกษา 2554 ที่ให้บริการในคลังปัญญาจุฬาฯ (CUIR)
เป็นแฟ้มข้อมูลของนิสิตเจ้าของวิทยานิพนธ์ ที่ส่งผ่านทางบัณฑิตวิทยาลัย
The abstract and full text of theses from the academic year 2011 in Chulalongkorn University Intellectual Repository (CUIR)
are the thesis authors' files submitted through the University Graduate School.

วิทยานิพนธ์นี้เป็นส่วนหนึ่งของการศึกษาตามหลักสูตรปริญญาวิศวกรรมศาสตรมหาบัณฑิต
สาขาวิชาวิศวกรรมไฟฟ้า ภาควิชาวิศวกรรมไฟฟ้า
คณะวิศวกรรมศาสตร์ จุฬาลงกรณ์มหาวิทยาลัย
ปีการศึกษา 2558
ลิขสิทธิ์ของจุฬาลงกรณ์มหาวิทยาลัย

FORMATION OF SUBCRITICAL THICKNESS InAs NANOSTRUCTURES ON InGaAs CROSS-HATCH PATTERNS BY IN SITU ANNEALING

Mr. Win Eiwwongcharoen

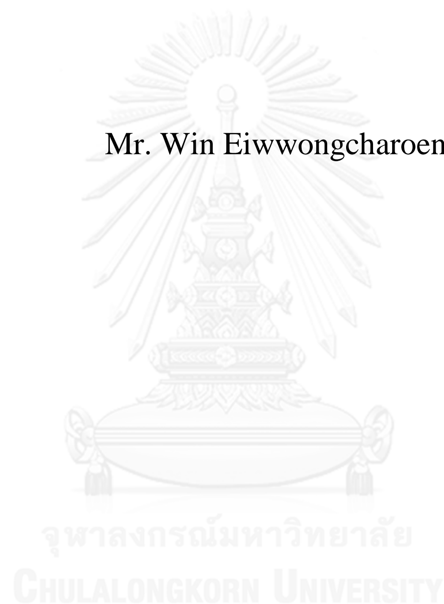

A Thesis Submitted in Partial Fulfillment of the Requirements
for the Degree of Master of Engineering Program in Electrical Engineering
Department of Electrical Engineering
Faculty of Engineering
Chulalongkorn University
Academic Year 2015
Copyright of Chulalongkorn University

Thesis Title	FORMATION OF SUBCRITICAL THICKNESS InAs NANOSTRUCTURES ON InGaAs CROSS-HATCH PATTERNS BY IN SITU ANNEALING
By	Mr. Win Eiwwongcharoen
Field of Study	Electrical Engineering
Thesis Advisor	Associate Professor Songphol Kanjanachuchai, Ph.D.

Accepted by the Faculty of Engineering, Chulalongkorn University in Partial Fulfillment of the Requirements for the Master's Degree

....Dean of the Faculty of Engineering
(Professor Bundhit Eua-arporn, Ph.D.)

THESIS COMMITTEE

....Chairman
(Professor Somsak Panyakaew, D.Eng.)

....Thesis Advisor
(Associate Professor Songphol Kanjanachuchai, Ph.D.)

....External Examiner
(Noppadon Nuntawong, Ph.D.)

จุฬาลงกรณ์มหาวิทยาลัย
Chulalongkorn University

วิน เอี้ยววงษ์เจริญ : การก่อตัวของโครงสร้างนาโนอินเดียมอาร์เซไนด์ที่บางกว่าความหนาวิกฤตบนแผ่นฐานลายตารางอินเดียมแกลเลียมอาร์เซไนด์โดยการแอนนีลแบบอินซิทู (FORMATION OF SUBCRITICAL THICKNESS InAs NANOSTRUCTURES ON InGaAs CROSS-HATCH PATTERNS BY IN SITU ANNEALING) อ.ที่ปรึกษาวิทยานิพนธ์หลัก: รศ. ดร. ทรงพล กาญจนชูชัย, 57 หน้า.

วิทยานิพนธ์ฉบับนี้นำเสนอการก่อตัวของโครงสร้างนาโน InAs ที่บางกว่าความหนาวิกฤตบนพื้นผิวลายตาราง $In_{0.2}Ga_{0.8}As$ ด้วยแผ่นฐาน GaAs (001) โดยการแอนนีลแบบอินซิทูในเครื่องปลูกผลึกด้วยลำโมเลกุล (Molecular Beam Epitaxy, MBE) การจัดเรียงตัวของโครงสร้าง InAs ที่บางกว่าความหนาวิกฤตถูกศึกษาการจัดเรียงตัวของผิวหน้าโดยกล้องจุลทรรศน์แรงอะตอม (Atomic Force Microscopy, AFM)

การสังเกตุผิวหน้าด้วยการมองภาพตามเวลาจริงไม่แสดงให้เห็นถึงการก่อตัวของควอนตัมดอตระหว่างการปลูกชั้นที่บางกว่าความหนาวิกฤต โดยผลลัพธ์ที่ได้จากการปลูกโครงสร้างนาโน InAs ที่บางกว่าความหนาวิกฤตบนพื้นผิวลายตาราง $In_{0.2}Ga_{0.8}As$ นั้นได้ผลที่น่าสนใจ ซึ่งเกิดเป็นขดลวดระดับอะตอมตามทิศ [1-10] ถ้าหากว่ามีการเปลี่ยนความหนาของชั้น InAs จาก 1.4 ไป 1.5 และ 1.6 ชั้นอะตอม (ML) ระยะห่างของขดลวดระดับอะตอมจะขยับเข้ามาใกล้กันมากขึ้น ส่งผลให้ขดลวดบนพื้นผิวนั้นมีความหนาแน่นมากขึ้น อย่างไรก็ตาม ความสูงของขดลวดนั้นได้ถูกพิจารณาว่ามีความสูงที่ใกล้เคียงกันหมด นั้นก็คือ 0.3 nm หรือเทียบเท่ากับความสูง 1 ML ของชั้น InAs

นอกจากนี้ พื้นผิวลายตารางยังส่งผลต่อการก่อตัวของชั้น InAs ที่บางกว่าความหนาวิกฤตทั้งทางทิศ [110] และ [1-10] โดยผลลัพธ์ที่ได้นั้นแสดงให้เห็นว่าโครงสร้าง InAs ที่บางกว่าความหนาวิกฤตนั้นมีแนวโน้มที่จะก่อตัวตามพื้นผิวลายตารางในทิศ [1-10] และจะถูกกักกันในทิศ [110] ในส่วนของการวัดผลเชิงแสงนั้นแสดงให้เห็นว่ามีค่ายอดพลังงานอยู่ที่ 1.45 eV ซึ่งสัมพันธ์กับชั้นฟิล์มบางของ InAs ซึ่งบ่งชี้ถึงโครงสร้างที่มีคุณภาพสูงที่อาจจะเหมาะสมกับการนำมาประยุกต์ใช้งานกับอุปกรณ์ทางแสงได้

ภาควิชา วิศวกรรมไฟฟ้า ลายมือชื่อนิสิต ....

สาขาวิชา วิศวกรรมไฟฟ้า ลายมือชื่อ อ.ที่ปรึกษาหลัก ....

ปีการศึกษา 2558

จุฬาลงกรณ์มหาวิทยาลัย
Chulalongkorn University

5670379321 : MAJOR ELECTRICAL ENGINEERING
KEYWORDS: INAS / INGAAS / CROSS-HATCH PATTERNS / IN SITU ANNEALING / SUBCRITICAL THICKNESS / AFM

WIN EIWWONGCHAROEN: FORMATION OF SUBCRITICAL THICKNESS InAs NANOSTRUCTURES ON InGaAs CROSS-HATCH PATTERNS BY IN SITU ANNEALING. ADVISOR: ASSOC. PROF. SONGPHOL KANJANACHUCHAI, Ph.D., 57 pp.

This thesis presents the formation of subcritical thickness InAs nanostructures on $In_{0.2}Ga_{0.8}As$ cross-hatch patterns (CHPs) with GaAs (001) substrate by *in situ* annealing in molecular beam epitaxy (MBE). The subcritical formation of InAs is characterized by atomic force microscopy (AFM) for surface morphology and topology.

The real time observation showed no sign of quantum dots (QDs) formation during the subcritical thickness. Subcritical thickness InAs nanostructures on $In_{0.2}Ga_{0.8}As$ CHPs show interesting nanostructures which formed into atomic wires along [1-10] direction. If varies the thickness of InAs layer from 1.4, 1.5, and 1.6 monolayer (ML), the distance between atomic wires become closer to each other, resulting in higher density of wires. However, the height of the wires is considered to be the same at 0.3 nm, which is equivalent to 1 ML of InAs layer.

Moreover, the CHPs also affect the formation of subcritical thickness InAs on both [110] and [1-10] directions as well. The results indicate that subcritical thickness InAs tends to elongate along [1-10] direction, and confined on the [110] direction. For the photoluminescence (PL) spectrum displays the highest PL peak at 1.45 eV, corresponding to the InAs wetting layer indicating a high structural quality which may be suitable for optical applications.

Department:	Electrical Engineering	Student's Signature ....
Field of Study:	Electrical Engineering	Advisor's Signature ....
Academic Year:	2015	

ACKNOWLEDGEMENTS

Firstly, I would like to express a sincere gratitude to my advisor, Associate Professor Dr. Songphol Kanjanachuchai, for his vision, guidance, and support, from the beginning until the the end of my Master Degree program. His suggestions are very useful in both researching and writing this thesis. Also, his knowledge that helped fix all the problems occurred to the system.

Besides my advisor, I would like to give thanks to my thesis committees: Professor Dr. Somsak Panyakeow and Dr. Noppadon Nuntawong, for their comments and questions that opened up new ideas and perspectives regarding to my research topic.

I also would like to thank Mr. Supachok Thainoi, Mr. Pornchai Changmoang, Mr. Pattana Phuntunwong, and Mrs. Kwanruan Thainoi, for their technical support and know-how knowledge. Without them, the system will not be able to operate correctly.

I thank all my friends for the warming friendship throughout my studied, for all the fun we have had in the last two-three years, and for the discussions that sparked new ideas related to my work. In particular, I am grateful to Mr. Nitas Nakareseisoon for all the collaboration during my research.

Finally, I would like to give special thanks to my family for encouraging support that motivated me to finish my Master Degree. Without them, I will not be here where I am now. Thank you all.

This research is funded by Thailand Research Fund (RSA5580015).

CONTENTS

Page

THAI ABSTRACT iv

ENGLISH ABSTRACT v

ACKNOWLEDGEMENTS vi

CONTENTS vii

LIST OF FIGURES x

LIST OF TABLES xiii

CHAPTER 1 Introduction 1

1.1 Historical Background 1

1.2 Objective 2

1.3 Overview 3

CHAPTER 2 Theoretical Background 4

2.1 Epitaxy 4

2.2 Nanostructures 5

2.2.1 Lattice Mismatch 6

2.2.2 Quantum Dots (QDs) 8

2.2.3 Dislocations 11

2.2.4 Cross-Hatch Patterns (CHPs) 13

Chapter 3 Experimental Details 15

3.1 *In Situ* Experiments 15

3.1.1 Molecular Beam Epitaxy (MBE) 15

3.1.2 Reflection High-Energy Electron Diffraction (RHEED) 18

3.2 Samples Preparation 19

3.2.1 Substrate Preparation 19

3.2.2 Pre-Heat Process 19

3.2.3 De-Gas Process 20

3.2.4 De-Oxidation Process 21

3.2.5 Surface Temperature Calibration 22

3.2.6 Growth Rate Calibration for GaAs 23

จุฬาลงกรณ์มหาวิทยาลัย
Chulalongkorn University

Page

3.2.7 Growth Rate Calibration for InAs 24
3.3 Growth Process 25
3.3.1 Buffer Layer 25
3.3.2 Cross-Hatch Patterns Layer 25
3.3.3 Quantum Dots and Subcritical Thickness Layer 26
3.4 *Ex Situ* Characterization 26
3.4.1 Atomic Force Microscopy (AFM) 26
3.4.2 Photoluminescence (PL) 27
Chapter 4 Results and Discussion 29
4.1 Summaries of Previous Works on Cross-Hatch Patterns 29
4.1.1 The Effects of Molar Fraction of In, x 30
4.1.2 The Effects of InGaAs Thickness, y 31
4.1.3 The Effects of Growth Interruption Time 31
4.1.4 Evolution of InAs Quantum Dots on Cross-Hatch Patterns, z 32
4.2 Subcritical Thickness Structures 33
4.2.1 Quantum Dots Formation in Subcritical Thickness 33
4.2.2 Complex Structure in Subcritical Thickness 34
4.2.3 Horizontal Nanowires in Subcritical Thickness 36
4.3 Surface Morphology of Subcritical Thickness InAs on Cross-Hatch Patterns 36
4.3.1 Surface Morphology of Annealed Samples 38
4.3.2 Surface Morphology of Non-Annealed Samples 40
4.3.3 Effects of Thickness for Subcritical Thickness InAs Layer 42
4.3.4 Effects of In Situ Annealing of Subcritical Thickness InAs Layer 43
4.3.5 Effects of Cross-Hatch Patterns on Subcritical Thickness InAs Layer 45
4.3.6 Effects of Long-Time Annealing on Subcritical Thickness InAs Layer 46
4.4 Optical Properties of Subcritical Thickness InAs on Cross-Hatch Patterns 47
4.4.1 Optical Properties of InAs QDs on Cross-Hatch Patterns 47
4.4.2 Optical Properties of Annealed Subcritical Thickness InAs on Cross-Hatch Patterns 48

จุฬาลงกรณ์มหาวิทยาลัย
CHULALONGKORN UNIVERSITY

Page

Chapter 5 Conclusions ... 50
REFERENCES ... 52
VITA ... 57

LIST OF FIGURES

Figure 2.1 Physical structure and density of state of (a) bulk, (b) quantum wells, (c) quantum wires or nanowires and (d) quantum dots [14]. 5

Figure 2.2 Graph representing energy band gap and lattice constant for various semiconductors. The indirect band gap materials are indicated by darker dots [19]. 7

Figure 2.3 Compressive strain formed by lattice mismatch between epitaxial layer and substrate [20]. 7

Figure 2.4 Equilibrium phase diagram in the function of thickness (H) and lattice mismatch (ε). Top and bottom panels illustrate the surface morphology in six different growth modes. The small white triangles indicate the stable islands and the big colored triangles indicate the ripened islands [21]. 8

Figure 2.5 Light emissions in (a) bulk and (b) quantum dot. 10

Figure 2.6 (a) The occurrence of misfit dislocation and threading dislocation that caused by the imperfection of boding atoms and (b) dislocation vectors of edge and screw dislocation [24]. 11

Figure 2.7 Mechanism of the formation of cross-hatch patterns [24]. 12

Figure 2.8 Graph representing relationship between H_c of InGaAs (ML) grown on GaAs and the molar fraction, x [27]. 14

Figure 3.1 RIBER 32P MBE system 16

Figure 3.2 Schematics of RIBER 32P growth chamber [29]. 17

Figure 3.3 Schematic representation of RHEED system [30]. 18

Figure 3.4 RHEED patterns of (a) streaky pattern, (b) de-ox pattern, and (c) spotty pattern, which indicate different surface state 19

Figure 3.5 Temperature profile for pre-heat process. 20

Figure 3.6 Temperature profile for de-gas process. 21

Figure 3.7 Temperature profile for de-ox process. 22

Figure 3.8 RHEED patterns during surface temperature calibration. Where (a) indicate flat surface before transition, (b) T_1, (c) T_2, (d) T_3, and (e) T_4, respectively. 23

Figure 3.9 (a) Formation of GaAs layer on GaAs(001) substrate. (b) The RHEED intensity related to the formation. And (c) the oscillation of specular beam during the GaAs deposition 24

Figure 3.10 (a) Seiko SPA-400 AFM machine. (b) Basic diagram of AFM. 27

Figure 3.11 Schematic of PL spectroscopy [29]. 28

Figure 4.1 Cross-sectional structure of CHPs experiments from previous generation. X, y, and z, indicated molar fraction, thickness of CHPs layer, and thickness of InAs layer, respectively. 30

Figure 4.2 AFM images of InAs QDs on 50 nm InGaAs CHPs, where the molar fraction is (a) 0.08, (b) 0.10, (c) 0.16, and (d) 0.20, respectively [34].. 30

Figure 4.3 AFM images of InAs QDs on $In_{0.15}Ga_{0.85}As$ with the thickness of (a) 50 nm, (b) 100 nm, and (c) 150 nm, respectively. The arrow is pointing to [1-10] direction [35]. 31

Figure 4.4 AFM images of InAs QDs on $In_{0.15}Ga_{0.85}As$ with GI time of (a) 0, ... 32

Figure 4.5 (a) AFM image of InAs QDs on $In_{0.2}Ga_{0.8}As$ CHPs with height contrast of 7.6 nm. And the images threshold with height contrast of (b) 5.5, (c) 4.9, (d) 4.0, and (e) 3.0 nm, respectively. The black color indicates the higher area and the white color indicates the lower area [34]. 32

Figure 4.6 TEM image of subcritical thickness InAs QDs at 1.4 ML grown on GaAs substrate [31]... 33

Figure 4.7 PL images of the density of (a) 1.3, (b) 1.4, and (c) 1.5 ML of InAs QDs grown on GaAs substrates [38]. 34

Figure 4.8 STM images of (a) InAs 1 ML with 30s GI, (b) InAs 1.5 ML with 30s GI, and (c) InAs 1.5 ML with 2s GI on singular GaAs(100) substrate. (d) A model of simple parquet structure for clarification [12]. 35

Figure 4.9 STM images of (a) InAs 1 ML with 30s GI and (b) InAs 1.5 ML with 2s GI on vicinal GaAs(100) substrate [12]. 35

Figure 4.10 AFM images of Ge HNWs on Si substrates with (a) high and (b) low density of Ge HNWs. (c) Ge HNWs with miscut angle. (d) 3D AFM image with cross-sectional image indicated in the inset [11]..... 36

Figure 4.11 Cross-sectional structures of (a) 1.6 ML, (b) 1.5 ML, and (c) 1.4 ML subcritical InAs layer on $In_{0.2}Ga_{0.8}As$ CHPs................................ 37

จุฬาลงกรณ์มหาวิทยาลัย
Chulalongkorn University

Figure 4.12 RHEED patterns for sample (a) A_16 with the inset showing (2 x *) surface reconstruction, (b) A_15, and (c) A_14 after the annealing process. 38

Figure 4.13 AFM images of (a)-(c) 5x5μm^2 and (d)-(f) 2x2μm^2 for sample A_16, A_15, and A_14, respectively. 39

Figure 4.14 RHEED patterns for sample (a) NA_16, (b) NA_15, and (c) NA_14 after subcritical thickness InAs deposition. 40

Figure 4.15 AFM images of (a)-(c) 5x5μm^2 and (d)-(f) 2x2μm^2 for sample NA_16, NA_15, and NA_14, respectively. 41

Figure 4.16 Surface morphology of 2x2μm^2 AFM images with line scan profiles of annealed sample (a) A_16, (b) A_15, and (c) A_14, respectively. 42

Figure 4.17 Surface morphology of 2x2μm^2 AFM images with line scan profiles of non-annealed sample (a) NA_16, (b) NA_15, and (c) NA_14, respectively. 44

Figure 4.18 Mean wire separation data with minimum and maximum values of both non-annealed (red) and annealed (green) samples with subcritical thickness InAs layer of 1.4, 1.5, and 1.6 ML, respectively. 45

Figure 4.19 (a) 5x5μm^2 AFM image of sample A_14 with (b) line scan profiles along [110] (pink) and [1-10] (blue) directions. 45

Figure 4.20 5x5μm^2 AFM images of (a) 1-hour-annealed with the inset of line scan of QDs and (b) 2-hour-annealed sample. Where (c) and (d) are line scan profiles for (a) and (b), respectively [42]. 46

Figure 4.21 (a) 2x2μm^2 AFM image of InAs QDs on $In_{0.2}Ga_{0.8}As$ CHPs with 6 nm of GaAs spacer and (b) the corresponding PL spectrum [43]. 48

Figure 4.22 The power dependent PL spectrum of sample A_15 without GaAs capping layer. 49

LIST OF TABLES

Table 1 Lattice constant and energy band gap of InAs, GaAs, and $In_xGa_{1-x}As$ [15] 6

Table 2 Overall procedures for each sample 37

CHAPTER 1

Introduction

1.1 Historical Background

Semiconductor technology is one of the most important inventions in the history of mankind. It has been playing a great role in modern age technology due to its electrical and optical properties. Semiconductor devices have been implemented into many kinds of optoelectronic devices, for example, photodetector [1], laser [2], transistor [3], light emitting diode (LED) [4], and solar cell [5].

Over the past few decades, semiconductor technology has been improved in many aspects, such as size and efficiency. The traditional semiconductor technology was dominated by silicon-based devices, because it is abundant in nature and easy to fabricate. However, the silicon-based devices have some limitations from the natural structure of the material, which is a single material or *homostructure.* To overcome such limitations, *heterostructure* semiconductor was introduced. *Heterostructure* is a structure that combines two or more materials together. In particular, a lot of optoelectronic devices are based on elements from group III combined with elements from group V in the periodic table. For example, gallium arsenide (GaAs) and indium arsenide (InAs), where Ga and In are from group III, and As is from group V.

Both *homostructure* and *heterostructure* can be synthesized by using a method called epitaxy. Epitaxy is a technique that grows a single crystal layer onto a substrate. There are three main methods for epitaxy: liquid phase epitaxy (LPE), chemical vapor epitaxy (CVE), and molecular beam epitaxy (MBE). MBE is the best research technique due to the accuracy of controlling the thickness of the epitaxial layer, which can be at the rate of monolayer per second (ML/s). At this rate, a small structure called nanostructure is form.

There are many kinds of nanostructures, such as quantum dots (QDs), quantum wires or nanowires (NWs), and quantum wells (QWs). These kinds of structures can be synthesized by two approaches: top-down or bottom-up approach. Both have their own advantages and disadvantages. The top-down approach is easier;

it enables to control the position of nanostructure by etching and lithography techniques that create patterns on the substrates, but it is difficult to control the size of nanostructure and also create defects on the surface [6]. On the other hand, the bottom-up approach is a self-assembled structure that formed by lattice mismatched between two materials at a certain thickness of epitaxial layer, called critical thickness. The size of nanostructure is more reliable compared to top-down approach, but occurred at random positions and random forms.

As mentioned above, the self-assembled process by the bottom-up approach is formed by the lattice mismatched between two materials at a critical thickness (h_c) of epitaxial layer. When the epitaxial layer reached h_c, a strain relaxation in materials occurred, this created three-dimensional (3D) islands, as known as QDs.

The random positions of nanostructures could be an issue that affects the efficiency in many devices [7], even though there are many other devices that do not require the alignment of nanostructures. Many researchers have tried to eliminate this issue by using misfit dislocation caused by lattice mismatched, known as cross-hatch patterns (CHPs). Several studies of CHPs with the growth of QDs through Stranski-Krastanow (SK) growth mode have shown the alignment of QDs [8-10], where they are very useful in applications like lasers and detectors.

A lot of attention is aimed toward nanostructures formed at h_c and beyond. However, very few are concerned about the intermediate stage or at subcritical thickness of epitaxial layer. At this stage, the results are still mysterious, but there are some studied that show interesting structures, such as NWs [11], parquet [12], and QDs [13]. In the case of QDs, the density of QDs is considered lower when compared to those formed at critical thickness.

1.2 Objective

The objective of this research is to study the formation of InAs nanostructures after *in situ* annealing in MBE system, where the thickness of InAs epitaxial layer is in the intermediate stage or at subcritical thickness. The structures are grown on InGaAs CHPs on GaAs(001) substrate. Also, the structural and optical properties will be analyzed.

1.3 Overview

This thesis is divided into 4 parts as follow: Theories and background knowledge about epitaxy and nanostructures are explained in chapter 2. Chapter 3 shows the experimental details and equipment that were used in this work, range from the epitaxy machine to the properties analysis equipment. All the data and results from this experiment are shown in chapter 4; including surface morphology by atomic force microscopy (AFM). Finally, all the data are summarized and concluded in chapter 5.

CHAPTER 2

Theoretical Background

This chapter explained the theories and background knowledge that are corresponded to this thesis; from epitaxy techniques to the fundamental of nanostructure. Also the formation nanostructure caused by the lattice mismatch, such as quantum dots (QDs) and dislocation.

2.1 Epitaxy

Epitaxy is a technique used principally to grow thin films of single crystal material onto a single crystal substrate, where the grown layer is called an epitaxial layer. This technique will produce high-quality crystal structures. The most well-known methods for epitaxy technique are categorized by the state of the substance, which can be divided into three main methods: liquid phase epitaxy (LPE), chemical vapor deposition (CVD), and molecular beam epitaxy (MBE).

The structure that grew by epitaxy technique can be either homoepitaxy or heteroepitaxy. Homoepitaxy is a process where epitaxial layer and substrate are the same material. The structure synthesized by this process is considered a lattice matched structure, where it is mostly used to obtain higher purity of the material or used to synthesis layers that have different doping level and/or type.

On the other hand, heteroepitaxy is an epitaxy process where epitaxial layer and substrate materials are different. This process can give either lattice matched or lattice mismatched structure, depending on the relative value of the lattice constants between the two materials. In the case of lattice matched, the nanostructure will form as 2D structure like the homoepitaxy process. In contrast, the lattice mismatched structure will form into different types of nanostructures, which have unique properties. Nanostructures that are formed by the lattice mismatched between two compound materials are explained later in this chapter.

2.2 Nanostructures

The prefix *nano* means *billionth*, which makes the word *nanometer* equals to *billionth of a meter.* When the material is reduces in size to the nanometer (nm) scale regime, the size of the material directly affects the energy band gap of the structure, which caused quantum confinement in the material. This quantum confinement determined both electrical and optical properties of the material, which is different than those in bulk materials. There unique properties can be applied for improvement over the bulk structure in many optoelectronic devices.

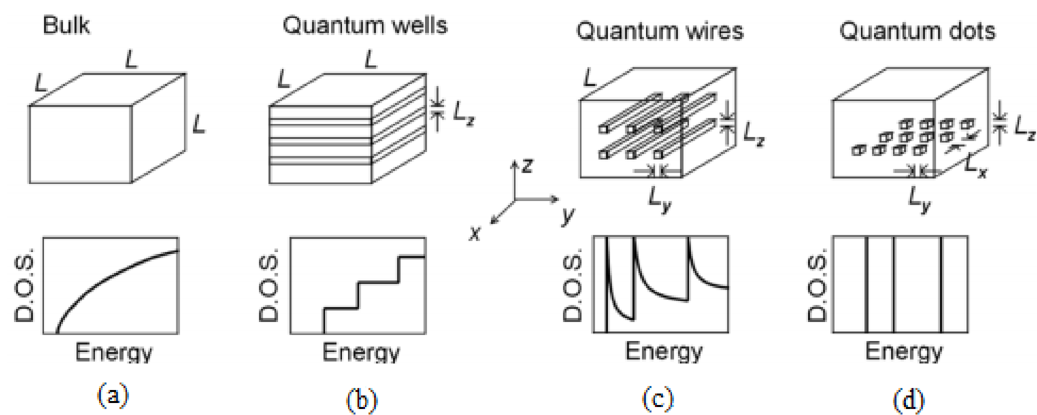

Figure 2.1 Physical structure and density of state of (a) bulk, (b) quantum wells, (c) quantum wires or nanowires and (d) quantum dots [14].

จุฬาลงกรณ์มหาวิทยาลัย
Chulalongkorn University

Figure 2.1(a) shows a physical structure for bulk, where the carrier can move in all three directions and has a continuous density of state (DOS) due to the larger size. While figures 2.1(b)-2.1(d) show semiconductor nanostructure, which can be divided into 3 kinds of structure: quantum well (QW), quantum wire or nanowire (NW), and quantum dot (QD).

QW is a nanostructure that has a carrier confinement in one direction, *z*-axis, which means that the carrier can move in two directions, *x*- and *y*-axis, with a stair-like DOS, shown in figure 2.1(b). Figure 2.1(c) illustrated NW structure, where the carrier can only move in one direction along the wire and has a discontinuous DOS. For QD, the structure is depicted by figure 2.1(d), where QD structure confined the carrier in all dimension, or considered as zero degree of freedom structure, and has DOS as a delta function.

2.2.1 Lattice Mismatch

Every element and compound material have their own value of lattice constant, *a.* The lattice constant of a crystal is a distance between two center atoms of the unit cell.

As mentioned before, if the epitaxial layer and substrate are the same material, it is called *homoepitaxy*, where the structure is lattice matched because they have the same lattice constant. On the other hand, *heteroepitaxy* can be either lattice matched or lattice mismatched depend on the lattice constant of the epitaxial layer and substrate.

Table 1 Lattice constant and energy band gap of InAs, GaAs, and $In_xGa_{1-x}As$ [15]

Materials	Lattice constant (Å)	Band gap (eV) at 300 K
InAs	6.0583	0.354
GaAs	5.6533	1.424
$In_xGa_{1-x}As$	5.6533+0.405(x)	$0.324+0.7(1-x)+0.41(1-x)^2$

In this thesis, the focus is aimed toward the structure formed by lattice mismatch, where the compound materials are InAs, GaAs, and $In_xGa_{1-x}As$. Table 1 shows the value of lattice constants and energy band gaps at 300K of these three compound materials. All the substrates that were used in this experiment were GaAs, where it has the smallest lattice constant compared to the other two compound materials.

There are many types of substrate that can be used with MBE machine, for instance InP [16], GaSb [17], and GaAs, which are from group III and V. There are also Si [11] and Ge [18], which are from group IV on the periodic table that can be grown with MBE system as well. However, according to figure 2.2, Si and Ge substrate are indirect band gap material, making them less suitable to use in optoelectronic devices. On the other hand, InAs and GaAs are direct band gap materials, which make them more suitable to use in optoelectronic devices. In addition, GaAs substrate is the cheapest III-V substrate in the market.

จุฬาลงกรณ์มหาวิทยาลัย
Chulalongkorn University

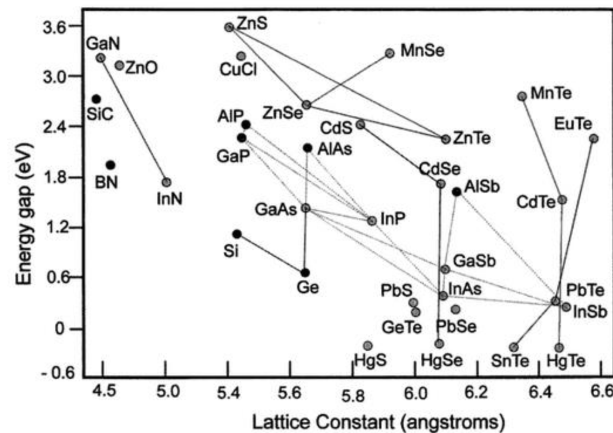

Figure 2.2 Graph representing energy band gap and lattice constant for various semiconductors. The indirect band gap materials are indicated by darker dots [19].

When the process is *heteroepitaxy*, the lattice constant between the epilayer and the substrate will create a strain between the materials. Strain can be divided into two types: compressive and tensile. Both compressive and tensile strains create a lattice deformation along the growth axis. Compressive strain occurred when the lattice constant in the substrate is smaller than that in the epitaxial layer. In contrast, tensile strain occurred when the lattice constant in the substrate is larger than that in the epitaxial layer. In the case of growing InAs and $In_xGa_{1-x}As$ on GaAs substrate, the compressive strain will occur, as shown in figure 2.3 below.

CHULALONGKORN UNIVERSITY

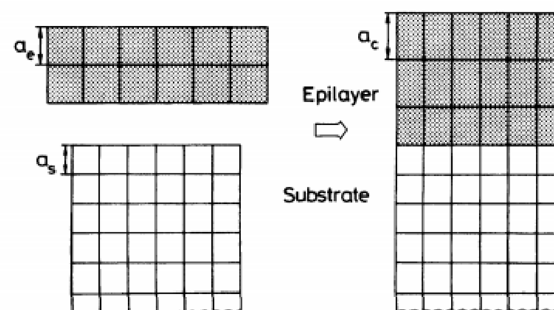

Figure 2.3 Compressive strain formed by lattice mismatch between epitaxial layer and substrate [20].

When the strain exceeds a certain thickness of deposition, called critical thickness (h_c), strain relaxation occurs. At h_c, strain relaxation will formed into 3D nanostructures, such as QDs or NWs. However, if the epitaxial layer has relatively

low strain, it will create defect between two layers instead. This defect leads to the dislocations that formed into cross-hatch patterns (CHPs) on the surface. The mechanism for these nanostructure formations is explained in the next section.

2.2.2 Quantum Dots (QDs)

The growth of an epitaxial layer onto the substrate can have different growth mode, which depends on the two main points: the lattice mismatch (ε) between two materials and the thickness of the epitaxial layer (H). The growth mode that occurred from the relationship between ε and H is shown in figure 2.4; it is divided into six different modes as follow:

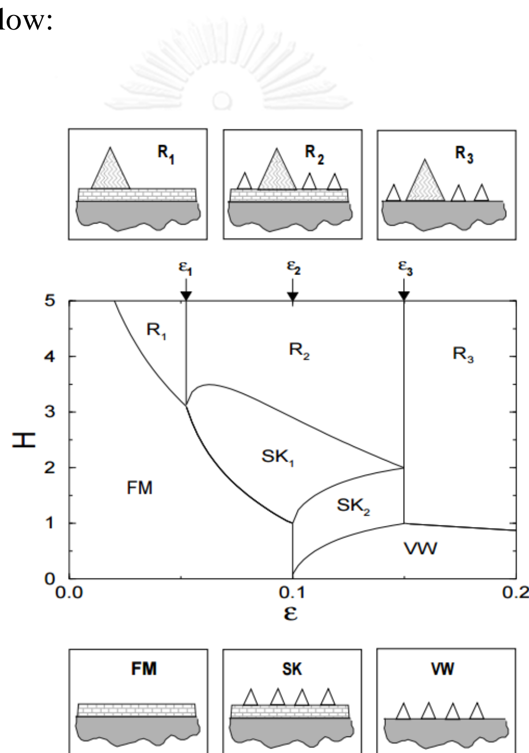

Figure 2.4 Equilibrium phase diagram in the function of thickness (H) and lattice mismatch (ε). Top and bottom panels illustrate the surface morphology in six different growth modes. The small white triangles indicate the stable islands and the big colored triangles indicate the ripened islands [21].

1. Frank-van de Merwe (FM) growth mode; this mode occurs when the epitaxial layer is grown layer by layer, which is considered as 2D growth mode, because the value of the lattice mismatch is low ($\varepsilon < 0.1$) and the thickness (H) is very small.

2. Volmer-Weber (VW) growth mode; this mode appears when the epitaxial layer becomes 3D islands due to the high lattice mismatch ($\varepsilon > 0.1$). The strain relaxation will instantaneously form the 3D islands.

3. Stranski-Krastanow (SK) growth mode; this mode is a mix between 2D (FM) and 3D (VW) modes. The value of the lattice mismatch in this mode falls between those of FM and VW growth mode ($0.05 < \varepsilon < 0.15$). SK can be sub-divided into two modes: SK_1 and SK_2. SK_1 growth mode occurs when the value of ε is close to that of FM growth mode. The initial state of this mode starts with 2D structure known as wetting layer (WL). When the thickness of the epitaxial layer grew thicker, the strain relaxation mechanism occurs and forms into 3D islands. On the other hand, SK_2 growth mode occurs when the value of ε is close to that of VM growth mode. The initial state of this mode starts with 3D islands structure. When the thickness of the epitaxial layer grew thicker, the 2D structure will form at an empty location where there are no 3D islands. At the end, the results for both SK_1 and SK_2 are the same, only different in the beginning approach.

4. R_1 growth mode; this mode causes by the lattice mismatch that has a value of less than 0.05 ($\varepsilon < 0.05$). It is a continuous process from FM growth mode, where the thickness of the epitaxial layer surpassed the critical thickness ($H > H_c(\varepsilon)$), the strain relaxation formed into 3D island that is larger than the one found in SK and VW growth mode, these island is called ripening island, and there is also WL as it is the initial state of FM growth mode.

5. R_2 growth mode; this mode causes by the lattice mismatch that has a value between 0.05 and 0.15 ($0.05 < \varepsilon < 0.15$). It is a continuous process from SK growth mode, which makes the 3D islands to become larger. There are also smaller 3D islands surrounding the larger one. WL is also found in this growth mode.

6. R_3 growth mode; this mode causes by the lattice mismatch that exceeds 0.15 ($\varepsilon > 0.15$). It is a continuous process from VW, where the additional layer creates smaller islands around the larger island. There is no WL in this growth mode.

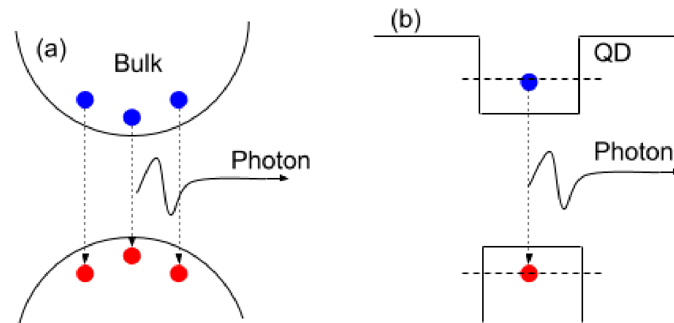

Figure 2.5 Light emissions in (a) bulk and (b) quantum dot.

QD has a physical structure that confine carrier, which makes the density of state to be discrete. This discreteness is called quantized states [22]. Due to the quantized states, QD emits light at a shorter wavelength when compared to those in bulk structure, which gives longer wavelength but lower intensity, illustrated in figure 2.5(a). In bulk structure, carriers can have higher energy than the conduction band (for electrons) and lower energy than the valence band (for hole), as shown in figure 2.5(b). This property makes the QD to be widely used in many kinds of optoelectronic devices. Furthermore, current technology can also be able to control the optical properties of the QD, such as wavelength and polarization, by optimizing the shape, the size, and the arrangement of QD.

In most case of InAs QDs, it is a self-assembled formation on the GaAs substrate due to the lattice mismatch between the two materials. InAs has a larger lattice constant than GaAs, which gives a compressive strain in InAs layer and formed into QDs. The lattice mismatch between epitaxial layer and substrate can be calculated by

$$\varepsilon = \frac{a_e - a_s}{a_s} \tag{2.1}$$

Where a_e is the lattice constant of the epitaxial layer and a_s is the lattice constant of the substrate. By using equation 2.1, the lattice mismatch between InAs and GaAs is

approximately ε = 0.072 or 7.2%, which falls in the SK growth mode according to figure 2.6. In theory, the critical thickness, h_c, for InAs epitaxial layer to form QDs is at 1.8 ML, but from the real world experiment concluded that it is form at 1.7 ML with the substrate temperature of 500°C.

2.2.3 Dislocations

Defects can be divided into four types: point defect, line defect, planar defect, and volume defect. In this thesis, the defect that leads to the formation of CHPs is line defect. The difference in the lattice constant between the epitaxial layer and the substrate creates strain that is caused by the imperfection of the alignment of bonding atoms. This imperfection is known as a misfit dislocation (MD).

In the case of growing $In_xGa_{1-x}As$ on GaAs substrate, MD will appear along the [110] and [1-10] directions. The density of MD is proportional to the molar fraction: *x* in $In_xGa_{1-x}As$ [23]. At every point of MD, there is another dislocation, which is line defect, called threading dislocation (TD). TD appeared in two directions: [001] and (111). Figure 2.6(a) shows TD that created along [001] direction is called a pure edge direction. On the other hand, TD that created along (111) is happened to form in a 60° angle, which is called 60° dislocation, as shown in figure 2.6(b). Most of TD is a chain reaction caused by two types of MD: edge dislocation and screw dislocation, which are the vectors in figure 2.4(b) denoted by b_{edge} and b_{screw}.

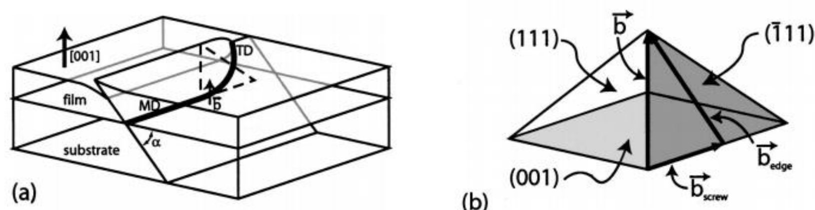

Figure 2.6 (a) The occurrence of misfit dislocation and threading dislocation that caused by the imperfection of boding atoms and (b) dislocation vectors of edge and screw dislocation [24].

According to the studied from M. Tamura et al. [25], the molar fraction that affects the TD formation can be defined into three ranges. The first range is when $x < 0.2$, all the TD will appear as a 60° dislocation. The second range is from $0.2 < x < 0.3$, TD will mix between a 60° dislocation and a pure edge dislocation. The third range occurred when $x > 0.3$, all the TD in this range is a pure edge dislocation.

TD is occurred by the gliding effect from the change in direction of MD. The easiest directions that TD can occurred are [1-10] and [110], because they are parallel to the MD [25]. The occurrence of TD starts from the MD and could go up to the topmost surface of the epitaxial layer. The directions [110] and [1-10] are perpendicular to each other and cross path at some points. With all the lines and cross sections, the TD creates a pattern that looks like cross-hatch, which is how the name cross-hatch pattern (CHP) has been realized. The optimal molar fraction for forming CHP is fall in the $x < 0.2$ range, which gives only a 60° dislocation and reduce the pure edge dislocation from occurring [26].

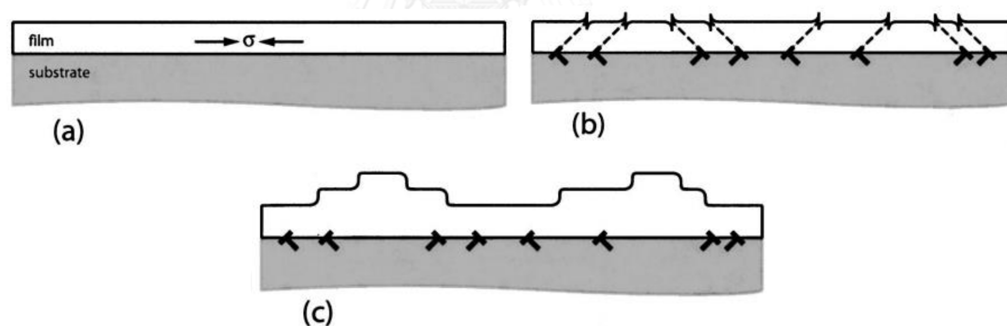

Figure 2.7 Mechanism of the formation of cross-hatch patterns [24].

Figure 2.7 shows the basic principle of surface evolution caused by the lattice mismatched materials that form into CHP. In figure 2.7(a), the initial state is considered as 2D structure before reaching H_c. When the thickness of epitaxial layer has reached H_c, the strain relaxation caused by MD creates TD from the points of MD to the surface, as shown in figure 2.7(b). The surface step on is then eliminated and formed into 3D pattern, shown in figure 2.7(c).

2.2.4 Cross-Hatch Patterns (CHPs)

Cross-Hatch Patterns (CHPs) are formed by the lattice mismatch between substrate and epitaxial layer with a value ~1.5% and 2 kinds of strains: compressive and tensile strain. The misfit and threading dislocation from the strain relaxation will appear on the surface in the form of cross hatch. CHP from group III-V compound materials, such as InGaAs on GaAs, will form in the orthogonal [1-10] and [110] directions [27].

The location of CHP will randomly occur, but the density of CHP can be adjusted with limitation. The adjustment can be done by vary the molar faction in $In_xGa_{1-x}As$ and the thickness of epitaxial layer. CHP forms when the epitaxial layer reach the H_c, where H_c is depend on the In molar faction and a 60° dislocation, which can be dictated by the following equations [15].

$$H_c = \frac{\frac{G_{GaAs}G_{InGaAs}b}{\pi(G_{GaAs}+G_{InGaAs})(1-v)}(1-v(cos\theta)^2)(\ln\left(\frac{h_{c60}}{b}\right)+1)}{Y_f} \quad (2.2)$$

When

$$G = C_{44} - \frac{1}{3}(2C_{44} + C_{12} + C_{11}) \quad (2.3)$$

$$b = \frac{\sqrt{2}}{2}a_{InGaAs} \quad (2.4)$$

จุฬาลงกรณ์มหาวิทยาลัย
Chulalongkorn University

$$v = \frac{C_{12}}{C_{12}+C_{11}} \quad (2.5)$$

$$Y = C_{11} + C_{12} + 2\frac{C_{12}^2}{C_{11}} \quad (2.6)$$

$$f = \frac{a_{InGaAs}-a_{GaAs}}{a_{InGaAs}} \quad (2.7)$$

Where v is the Poisson ratio, G is the anisotropic factor, C is the elastic constant and Y is the Young's modulus of elastic constant. If the molar faction of In is 0.2, the value of H_c = 6 nm as shown in figure 2.8 below.

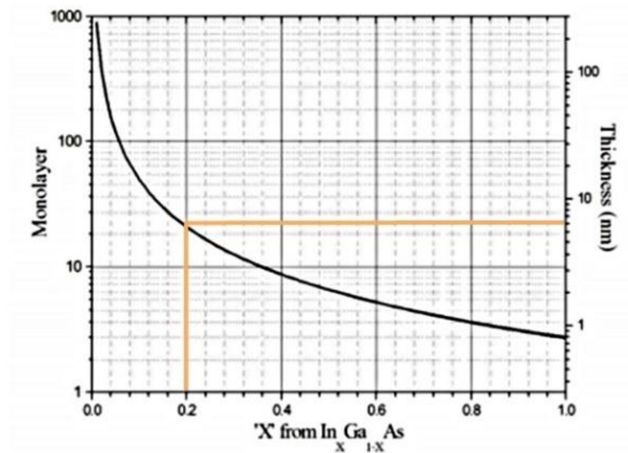

Figure 2.8 Graph representing relationship between H_c of InGaAs (ML) grown on GaAs and the molar fraction, x [27].

In InGaAs/GaAs CHP, the CHP on [1-10] will be higher than on [110] direction, because the dominant material in [1-10] is As and for [110] is Ga. So the appropriate molar faction for InGaAs and the right amount of thickness, will create CHP along [1-10] more than [110] direction [28].

จุฬาลงกรณ์มหาวิทยาลัย
Chulalongkorn University

Chapter 3

Experimental Details

This chapter explains the experimental details used to grow and characterize all the samples in this thesis. The contents in this chapter are divided into 4 sections. Section 3.1 explains the *in situ* experiments, which includes molecular beam epitaxy (MBE) machine and reflection high-electron energy diffraction (RHEED) observation. Section 3.2 explains the samples preparation process performed in this experiment. Section 3.3 explains the growth processes for all the samples in this thesis. And section 3.4 explains the *ex situ* characterization, including atomic force microscopy (AFM) and photoluminescence (PL) for surface characterization and optical characterization, respectively.

3.1 *In Situ* Experiments

3.1.1 Molecular Beam Epitaxy (MBE)

The epitaxial growth method is a method that grows a layer of single crystal material onto a substrate that is also a single crystal material. There are many methods for epitaxial growth, such as liquid phase epitaxy (LPE), vapor phase epitaxy (VPE), and molecular beam epitaxy (MBE). Each has their own advantages and disadvantages, but the most widely used method is MBE, due to the accuracy in the epitaxial growth. MBE can grow an epitaxial layer at the rate of monolayer per second (ML/s) and operates under high vacuum environment and is thus suitable for optoelectronics that need very high quality and purity materials.

All the samples in this thesis experiment were grown on GaAs substrate by using MBE technique. The MBE machine that was used to grow is RIBER 32P. The MBE system consists of four chambers: loading chamber, introduction chamber, transfer chamber, and growth chamber. Each chamber is separated by a gate valve, which make the pressure inside of the chamber to be independent from each other, as shown in figure 3.1.

จุฬาลงกรณ์มหาวิทยาลัย
CHULALONGKORN UNIVERSITY

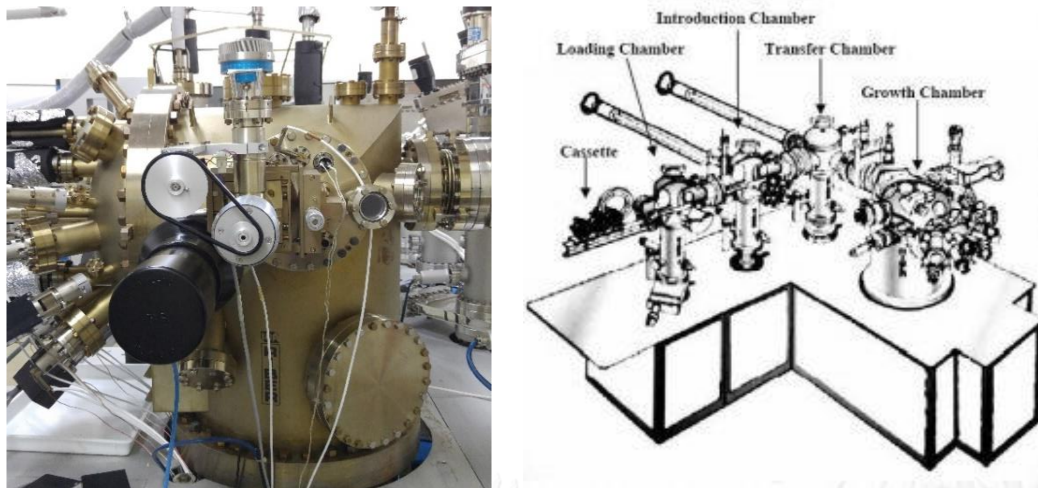

Figure 3.1 RIBER 32P MBE system

1. Loading chamber; this is the entry chamber that is simply use for loading samples in and out. This is the only chamber that makes contact to both vacuum and atmosphere (1 atm or 760 Torr) environment. Loading chamber is connected to the introduction chamber, which will be explained later. There are four components for loading chamber: main gate, nitrogen valve, turbo pump valve, and a gate that separated loading chamber and introduction chamber.

To change the pressure in loading form vacuum to atmospheric, nitrogen gas is needed to increase the pressure inside the loading chamber. Before open the nitrogen gas valve, other gates and valves must be tightly closed to prevent leakage. On the other hand, to change the pressure in loading chamber from atmospheric to vacuum for loading the samples in, the diaphragm pump is needed to reduce the pressure inside loading chamber down to 1 Torr. Then, the turbo pump is turned on to reduce the pressure to $5x10^{-6}$ Torr before the gate that separates loading chamber and introduction chamber can be open.

2. Introduction chamber; this chamber is use to pre-heat the sample. The pre-heat process to clean the surface of the sample. A tool called magnetic arm is used to move the sample in and out of the pre-heat station. After pre-heated, the sample will be transferred into the transfer chamber. In introduction chamber, the ion pump and titanium pump is always on to trap the contamination that came out from the surface during the pre-heat process and reduce the pressure inside the chamber.

3. Transfer chamber; this is where the samples are being stored after or waiting for the pre-heat process. This chamber is also a buffer chamber that separates the introduction chamber from the growth chamber, because during the pre-heat process, the pressure in the introduction chamber will rise due to the contamination that came out from the surface of the sample. There is also another magnetic arm in the transfer chamber for transferring samples in and out of the growth chamber.

4. Growth chamber; this is where the epitaxy process takes place. It is the biggest chamber compared to the other three chambers. The pressure inside of growth chamber must be lower than 10^{-9} Torr. The always-on ion pump and titanium pump are used to traps all the contamination inside the growth chamber, where titanium pump is turned on only when the system is not in use.

The growth chamber consists of over manipulator (OM), ion pump, titanium pump, and RHEED. The back of the growth chamber is filled with effusion cells that contain materials loaded into crucibles. This specific RIBER 32P MBE system contains only materials from group III and V, plus the exception of Si cell.

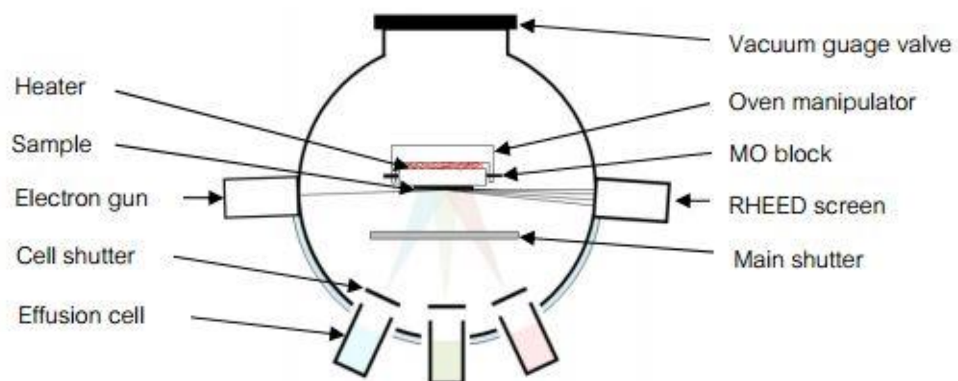

Figure 3.2 Schematics of RIBER 32P growth chamber [29].

The samples are held by the OM that has a heater to heat up the sample during growth, which can also be rotated by using direct-current (DC) motor so that the molecular beams will hit the surface of the samples thoroughly. Before the growth, the main shutter that separated the growth chamber and crucibles is close to prevent any contamination. There is also shutter for each effusion cells. The amount of epitaxial layer is controlled by the temperature in crucible. Higher temperature means

higher rate of epitaxial layer and also higher pressure. The rate of growth for each compound material can be calculated by observing the change of the surface reconstruction using RHEED.

3.1.2 Reflection High-Energy Electron Diffraction (RHEED)

The deposition rate during the growth in MBE machine is very crucial. Real time observation is needed to calibrate the deposition rate. RHEED is the tool that is used to observe real time surface reconstruction. The principle of RHEED is shown in figure 3.3, where the electron gun shoots a focused beam of electrons onto the surface's sample and reflects to the fluorescent or phosphor screen on the other end.

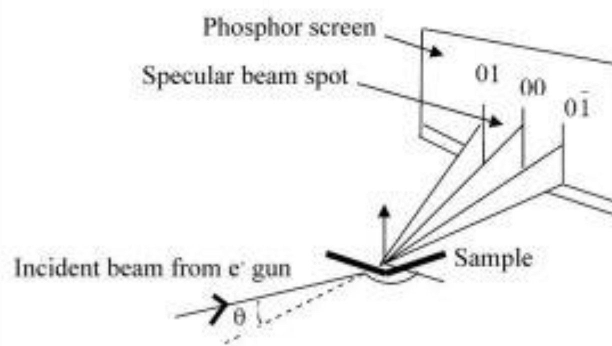

Figure 3.3 Schematic representation of RHEED system [30].

RHEED patterns that display on the phosphor screen show different surface states. But the three most important patterns that are needed for growth rate calibration are streaky, de-ox, and spotty patterns. The streaky pattern indicates the flatness of the surface, as shown in figure 3.4(a). Figure 3.4(b) presents the pattern when the surface reached the de-oxidation temperature. Where spotty pattern indicates the 3D islands formation on the surface, as shown in figure 3.4(c).

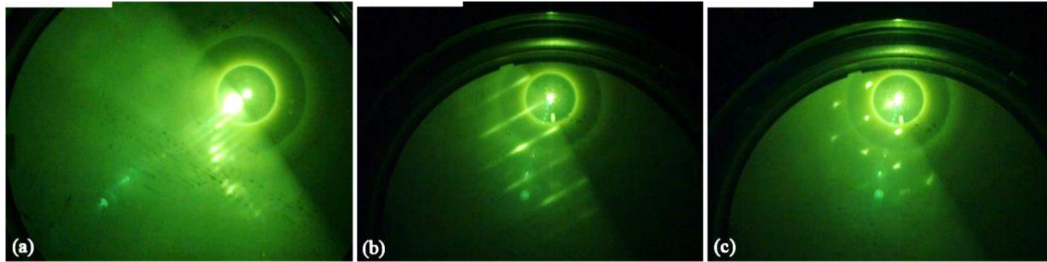

Figure 3.4 RHEED patterns of (a) streaky pattern, (b) de-ox pattern, and (c) spotty pattern, which indicate different surface state.

3.2 Samples Preparation

Every sample has the same pre-process before growing process, which is also a very important procedure that has to be strictly followed. If the pre-process is skipped or not properly carried out, the samples might fail or get the misguided results. The samples preparation can be divided into substrate preparation, pre-heat process, de-gas process, de-oxidation process, surface temperature calibration, and growth rate calibration for GaAs and InAs.

3.2.1 Substrate Preparation

Substrates are cut from single crystal GaAs wafer into smaller pieces and stick to the Molybdenum block (Mo block) by using In glue. The In glue is applied onto the Mo block that is rested on the heater with temperature between 250-270 °C. When In glue has melted, the substrate is then applied onto the In glue and being push back and forward to distribute the In glue underneath. This procedure is very important because it will help the heat distribution throughout the sample. After the substrate is properly mounted on the Mo block, the block then will be transferred from the heater to let it cool down for a little bit before cleaning the left-over In glue on the side.

3.2.2 Pre-Heat Process

Pre-heat process is a process that gets rid of the water vapor from the surface. This water vapor contains contamination when it was exposed to the atmosphere before transferring into the vacuum environment. Although, the pre-heat process is to clean the surface, but it does not remove surface oxides.

This process is done in the introduction chamber. The process begins by transferring the sample to the pre-heat station using the magnetic arm. The temperature is then ramped up from 30°C to 450°C in 1 hour. When the temperature reaches 450°C, it will stay there for 1 more hour. After that, the temperature will be ramped down again to 30°C in 1 hour. The whole pre-heat process takes 3 hours, as shown in figure 3.5. When the contamination is being removed from the surface, the pressure inside the introduction chamber will increase. To reduce the pressure, the ion pump is used to suck out the contamination out of the chamber.

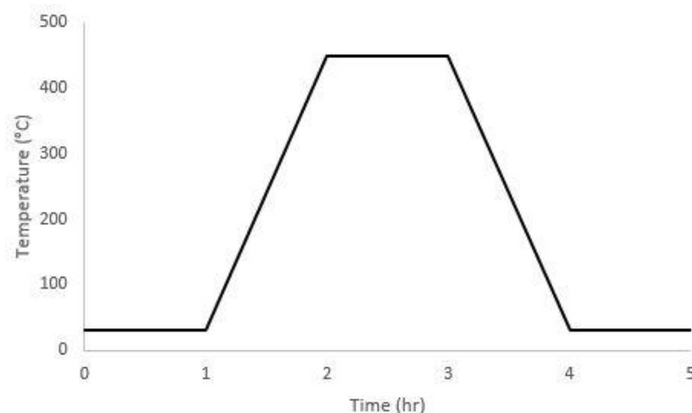

Figure 3.5 Temperature profile for pre-heat process.

3.2.3 De-Gas Process

After the pre-heat process is completed, the sample is transferred from the introduction chamber to the transfer chamber, and then to the growth chamber. Before starting the growth process, the effusion cells for group III materials, In and Ga, need to be cleaned first. This process is called de-gas process. Figure 3.6 shows the temperature profile for de-gas process, where it is done by ramping up the temperature of effusion cells to 50°C above the highest temperature that will be used in that experiment. The ramping rate for both cells is 30°C per minute. When the temperature reaches the setting temperature, the shutter for both cells will be open for 5 minutes but the main shutter remains close. The contamination inside each cell will evaporate out. After de-gas period ends, the shutters of effusion cells will be closed and the cell temperatures are reduced to operating temperatures.

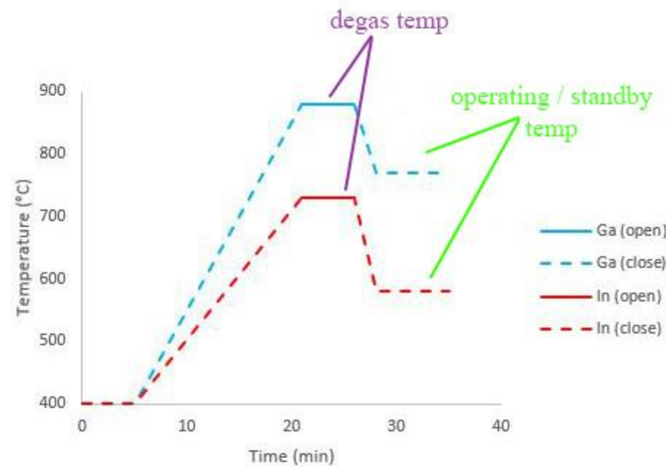

Figure 3.6 Temperature profile for de-gas process.

3.2.4 De-Oxidation Process

The process after de-gas process is called de-oxidation or de-ox process. In this process, As cell is ramped up to an appropriate value with the rate of 5°C per minute. At the same time, the OM temperature is ramped up to 300°C. When both temperatures reaches the setting points, the shutter of As cell and the main shutter will be open at the same time to let the As_4 flux fill in the growth chamber. When the pressure is stable, the OM temperature will be ramped up with the rate of 30°C per minute to begin the de-ox process.

De-ox process is a process that removes the surface oxide, which couldn't be removed by the pre-heat process. Due to the high temperature, As tends to evaporate out of the surface and Ga droplets can be formed unless high As_4 pressure is present. The theoretical temperature for de-oxidation is 580°C. So when the temperature is closer to the de-ox temperature, the ramping rate is reduced to 10°C per minute and the observation RHEED pattern begins here. After de-ox pattern is shown on RHEED screen, the temperature is then ramped up to 30°C above the de-ox temperature and kept there for 20 minutes to remove the surface oxide as much as possible. The temperature profile for de-ox process is shown in figure 3.7. The de-ox temperature is often denoted as $T_{de\text{-}ox}$. $T_{de\text{-}ox}$ is also used for growing buffer layer.

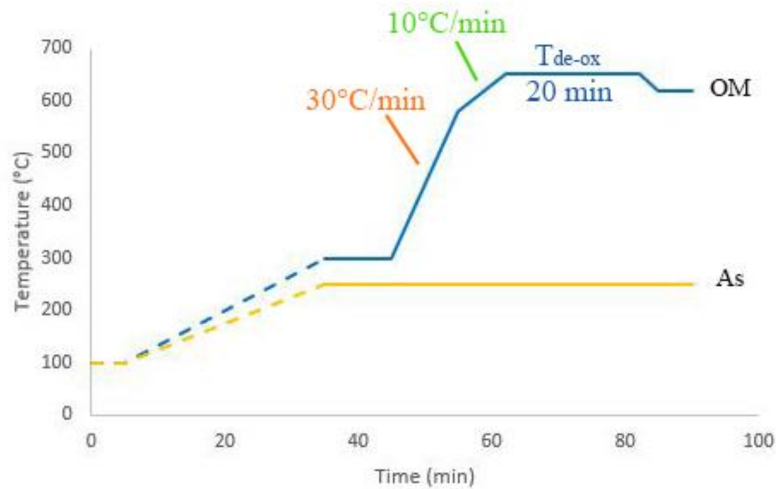

Figure 3.7 Temperature profile for de-ox process.

3.2.5 Surface Temperature Calibration

The theoretical temperature for the growth process is around 500°C. However, the actual surface temperature is difference. To find the actual surface temperature, the correlation between the OM temperature and the change in RHEED pattern are needed. The motor is stopped at [1-10] direction of the surface, which illustrated 5 lines on the RHEED screen, which is a (2x4) pattern, to observe the RHEED pattern revolution. Figure 3.8 shows the RHEED patterns for surface temperature calibration. The temperature of OM is ramped down with the rate of 10°C per minute until the middle line is disappeared, which denoted as T_1. When the temperature goes lower, the appearance of the middle line is denoted as T_2. T_3 and T_4 have the same mechanism as T_1 and T_2, but the temperature is increase instead of decrease. The average of T_1, T_2, T_3, and T_4 is called transition temperature ($T_{transition}$), which is the growth temperature for that experiment, and theoretically defined to be 500°C.

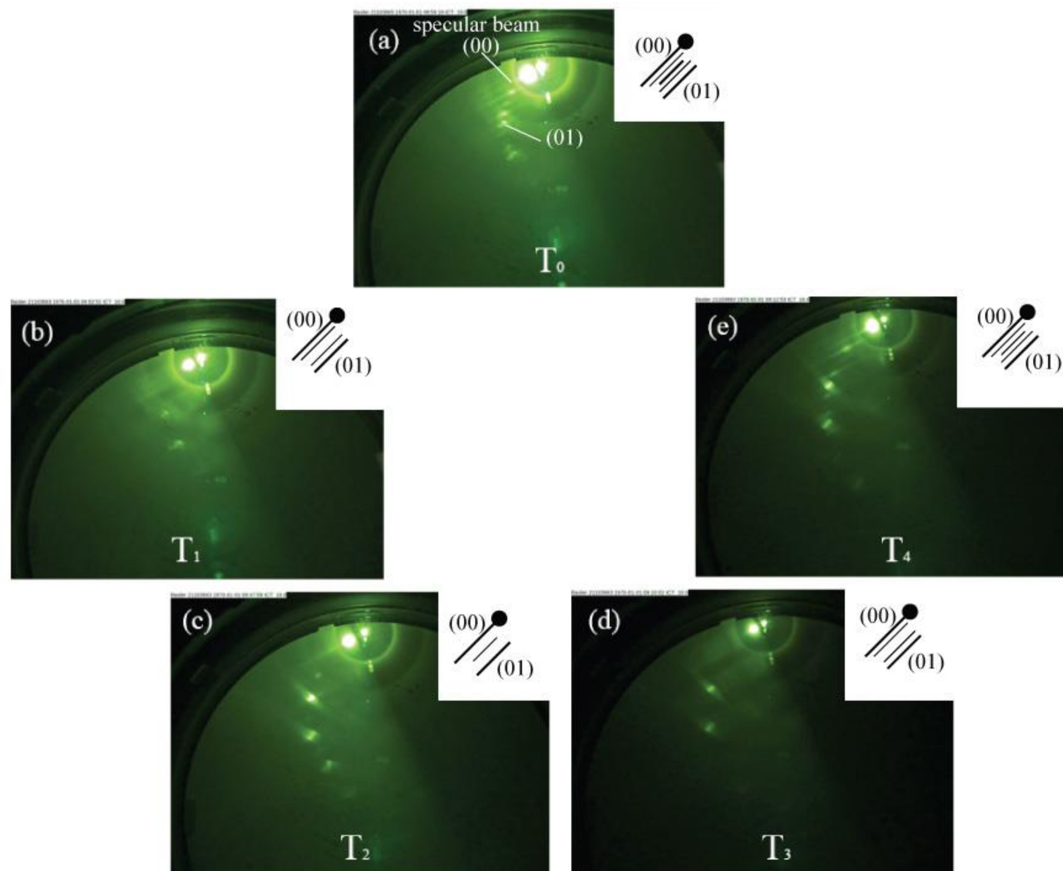

Figure 3.8 RHEED patterns during surface temperature calibration. Where (a) indicate flat surface before transition, (b) T_1, (c) T_2, (d) T_3, and (e) T_4, respectively.

จุฬาลงกรณ์มหาวิทยาลัย
Chulalongkorn University

3.2.6 Growth Rate Calibration for GaAs

In this experiment, GaAs is used for growing buffer layer, spacer layer, and also part of the InGaAs CHPs. The calibration of GaAs is started by setting the OM temperature to $T_{transition}$ and ramped Ga cell to the setting temperature. The DC motor is stopped to observe the revolution of specular beam on the RHEED pattern. When the Ga shutter is opened, the oscillation of the specular beam from brightest to darkest is considered as 1 cycle, which is equal to 1 ML of GaAs. Figure 3.9 illustrates the formation and specular beam oscillation during the deposition of GaAs layer on the GaAs(001) substrate. The growth rate of GaAs is calculated by the cycle divided by time, which is in the unit of ML/s. After obtained the desired growth rate, the surface is flattened by growing GaAs layer for 20 nm.

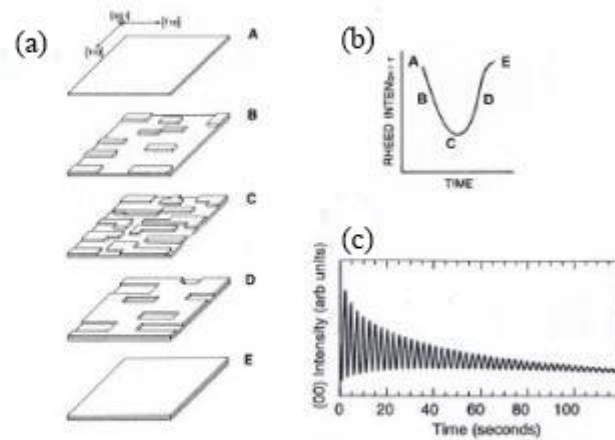

Figure 3.9 (a) Formation of GaAs layer on GaAs(001) substrate. (b) The RHEED intensity related to the formation. And (c) the oscillation of specular beam during the GaAs deposition

3.2.7 Growth Rate Calibration for InAs

InAs is used for growing subcritical thickness in this experiment and also part of the InGaAs CHPs. The h_c of InAs on GaAs is at 1.7 ML, while the lattice mismatch between InAs and GaAs is approximately 7.2%. The calibration of InAs is started by setting OM temperature to $T_{transition}$ and ramped In cell to the setting temperature. The DC motor is kept in motion to observe the revolution of the RHEED pattern. When In shutter is open, the RHEED pattern will change when reached h_c, from streaky patterns to spotty patterns. The change in the pattern indicates the 3D islands formation on the surface. The growth rate of InAs is calculated by taking 1.7 ML and divided by the time that the spotty pattern appeared, which is in the unit of ML/s.

However, the calibration of InAs left the 3D islands on the surface. To get rid of the 3D islands, the OM temperature is ramped up to $T_{de\text{-}ox}$ to evaporate the InAs from the GaAs. When InAs 3D islands have been evaporated, the surface of the sample will be rough. GaAs buffer layer of at least 100 nm is grown on top to flatten the surface before further experimentation.

3.3 Growth Process

The growth process for III-V compound materials semiconductor in this thesis contains 3 difference layers: buffer, CHPs, QDs and subcritical thickness layer. The QDs layer is only for InAs calibration purpose, so it is grouped with the subcritical thickness layer.

3.3.1 Buffer Layer

Buffer layer is the layer used for flattening the surface of the sample before and after the InAs calibration and evaporation. It is the thickest layer and is lattice matched with the substrate, in this case GaAs on GaAs. Furthermore, the buffer layer is also GaAs buffer layer, where it is grown after the de-ox process at the substrate temperature of 580°C. The thickness of the GaAs buffer layer is approximately 100 nm. For convenient, the GaAs buffer layer is grown at the rate of 0.6 ML/s, which is converted to approximately 10 minutes.

3.3.2 Cross-Hatch Patterns Layer

Cross-hatch patterns (CHPs) are occurred by the lattice mismatched between substrate and epilayer as mentioned in the previous chapter. The compound material for CHPs in this thesis is $In_xGa_{1-x}As/GaAs$, where the lattice constant for CHPs is proportional to the molar faction, *x*. To form the CHPs, the lattice mismatch should not be too large, to prevent the formation of 3D islands. The dislocation for zinc blend structure, such as InGaAs, is easily occur along [1-10] and [110] direction.

To grow InGaAs CHPs, the shutter for both In and Ga are open at the same time. The molar fraction of In should not be higher than 20% to prevent 3D islands formation. In this particular experiment, the molar fraction is $In_{0.2}Ga_{0.8}As$. When both shutters are opened, In and Ga molecules react with As_4 in the growth chamber and form CHPs when reached critical thickness for dislocation formation in InGaAs/GaAs, H_c, as shown in figure 2.8.

3.3.3 Quantum Dots and Subcritical Thickness Layer

QDs and subcritical thickness layer have the same process but difference in the layer thickness. For QDs, the first few layers are arranged in 2D manners similar to quantum wells, called wetting layer (WL). When the thickness reached critical thickness for QD formation in InAs/GaAs, h_c, the 3D islands will form according to SK growth mode, as shown in figure 2.4. However, in this thesis, QDs layer is only for InAs calibration purpose. On the other hand, the thickness of subcritical layer is below the h_c, which is considered as WL and falls into FM growth mode.

The h_c of InAs for QDs to form on GaAs is 1.7 ML, which make the subcritical thickness to be 1.6 ML and below. In this thesis, the subcritical thicknesses range from 1.4-1.6 ML. For QDs, RHEED pattern will change to spotty pattern, which indicated the 3D islands formation. On the other hand, RHEED pattern for subcritical thickness will not change during the growth because there is no 2D-to-3D transition.

3.4 *Ex Situ* Characterization

Since RHEED images during the growth process do not show a clear picture of the surface reconstruction, the *ex situ* tools are needed to observe the morphology of the samples. In this experiments, atomic force microscopy (AFM) is used to see the surface topography. Where, photoluminescence (PL) spectroscopy is used to analyze the optical properties of the samples.

3.4.1 Atomic Force Microscopy (AFM)

To observe the topography of the sample, AFM is introduced. AFM is a machine that analyzes the structure of the surface in the size of nanometer scale. AFM can be divided into 3 modes: contact-mode, non-contact mode, and tapping mode. The system consists of tip, cantilever spring, laser, and photodetector. In this experiment, the samples were measured using Seiko SPA-400 AFM machine operated by dynamic mode, which is equivalent to tapping mode in typical AFM system. Figure 3.10 shows the Seiko SPA-400 AFM machine and a basic diagram of AFM.

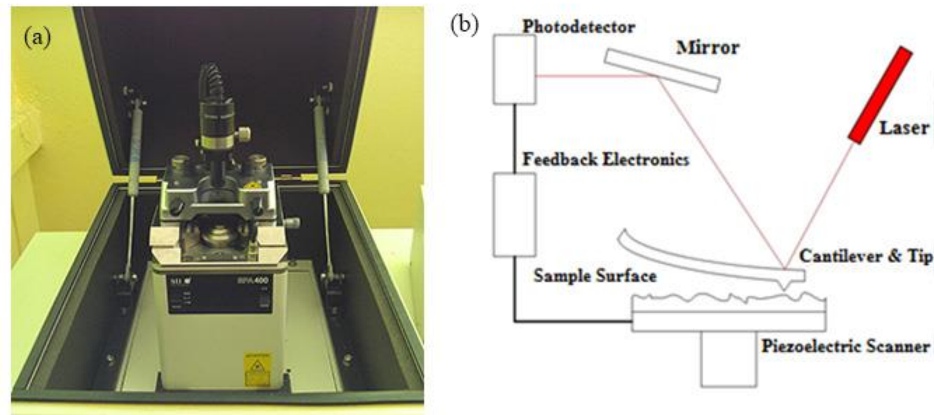

Figure 3.10 (a) Seiko SPA-400 AFM machine. (b) Basic diagram of AFM.

The system starts with the movement of the tip on the cantilever spring over the surface of the sample, where the oscillation is kept constant. When the tip moves in x and y direction, the z direction will move up and down corresponding to the surface of the sample due to the electromagnetic force. During the movement of the cantilever, the laser is shone onto the cantilever, and then the reflection of the laser is detected by the photodetector and displays 3D images on the computer corresponding to the cantilever's motion

3.4.2 Photoluminescence (PL)

Direct band gap semiconductor can release photon energy when excited by light with higher energy band gap. Each released photon has different wavelength than each other, which is depend on the unique properties of the sample. The technique that is used to measure the photon intensity is called photoluminescence (PL) spectroscopy.

The PL spectroscopy started by shining an Ar^+ laser, with a wavelength of 514.5 nm, through a chopper to convert a signal from DC to AC with the frequency of 330 Hz. The conversion is done to reduce the noise from the 50 Hz generator. Then the laser beam will go through a collector lens, which reduces the diameter of the beam but increase in intensity. The sample is placed in a vacuum container, called cryostat. The collected laser beam that hit the sample has an energy of 2.6 eV (476.5 nm), which is higher than the energy band gap of GaAs sample, 1.43 eV at 300K or

1.52 eV at 20K, respectively. The schematic of PL spectroscopy is shown in figure 3.11.

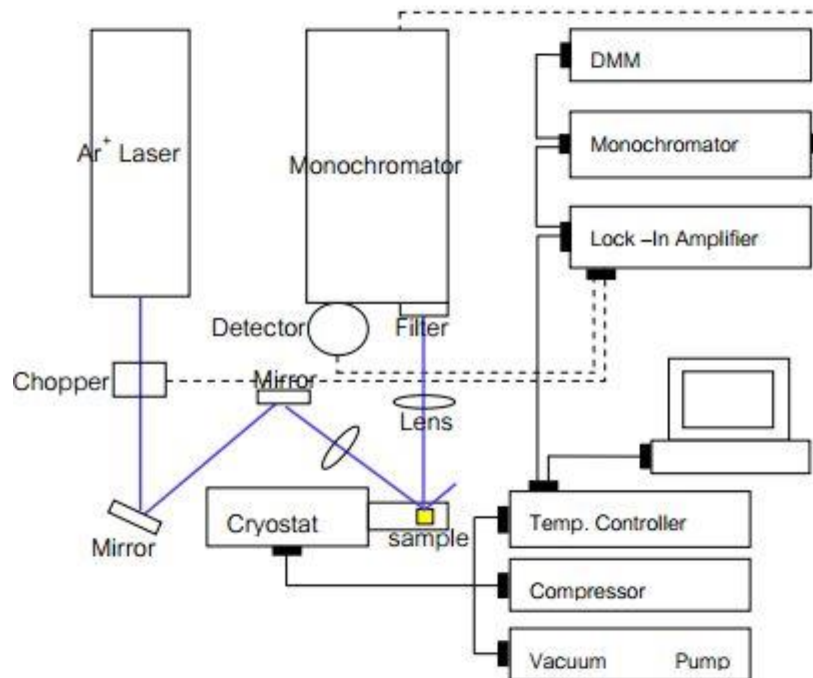

Figure 3.11 Schematic of PL spectroscopy [29].

When the laser beam hit the sample, the sample will absorb the energy and create an electron-hole pair, and then electron will recombine with hole. During the recombination, the energy difference will emit energy that depends on the type of energy band gap of the structure. For direct bang gap semiconductor, the sample will release its energy in the form of photon. On the other hand, indirect band gap semiconductor will release its energy in the form of phonon. The emitted photons are collected by the monochromator, which screens photons with various wavelengths and selects wavelength that fall in the wanted range.

In this experiment, the PL measurement is done with a power dependent technique, which varied laser power but keep a constant temperature at 20K. The samples were measured without a GaAs capping layer on top to studied optical properties of uncapped InAs surface structures

Chapter 4

Results and Discussion

The main focus for this thesis is to study the formation of subcritical thickness of InAs layer on InGaAs cross-hatch patterns by *in situ* annealing and analyze the characteristic of the nanostructure. This chapter reports the results from the experiments, which can be divided into 3 sections. Section 4.1 presents the summaries of the previous works that have been done with InGaAs cross-hatch patterns. Section 4.2 reviews the relevant results with the subcritical thickness nanostructures. In Section 4.3, the results from this thesis are presented, including surface morphology and topology of subcritical InAs layer on $In_{0.2}Ga_{0.8}As$ CHPs. Finally, Section 4.4 explains the optical properties of subcritical thickness InAs layer without GaAs capping layer.

With the vast attention devoted to the formation of QDs due to the unique properties of the structure in both electrical and optical; the formation of subcritical thickness nanostructures are still poorly understood. However, few studies have shown some interesting nanostructures obtained from the subcritical thickness layer, such as HNWs [11], low density QDs [31], and complex parquet structure [12]. There are many applications in optoelectronic devices for these kinds of nanostructures, such as nanosensors [32], fiber-based communication [33], and many more.

4.1 Summaries of Previous Works on Cross-Hatch Patterns

The previous works that have been done on InGaAs CHPs were mostly QDs structure on CHPs. The cross-sectional structure is shown in figure 4.1. The substrate is GaAs (001) and flattened by 300 nm of GaAs buffer layer, followed by InGaAs CHPs. Then, InAs layer is grown on top of InGaAs CHPs. The variables *x, y* and *z* are the molar fraction of In, the thickness of CHPs, and the evolution of InAs layer on InGaAs CHPs, respectively.

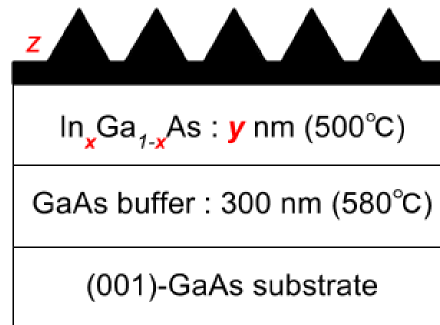

Figure 4.1 Cross-sectional structure of CHPs experiments from previous generation. X, y, and z, indicated molar fraction, thickness of CHPs layer, and thickness of InAs layer, respectively.

4.1.1 The Effects of Molar Fraction of In, *x*

The cross-hatch density for InGaAs CHPs is directly depends on the molar fraction of In, *x*. When the value of *x* increases, the density of CHPs and QDs are also increase. This natural phenomenon can be explained by the strain relaxation during the growth of InGaAs. According to table 2.1, the higher value of *x* causes the lattice constant of $In_xGa_{x-1}As$ to become larger. Thus, the H_c for dislocations becomes lower. So the MD and TD occurred faster at higher value of *x*, which result in higher density of CHPs.

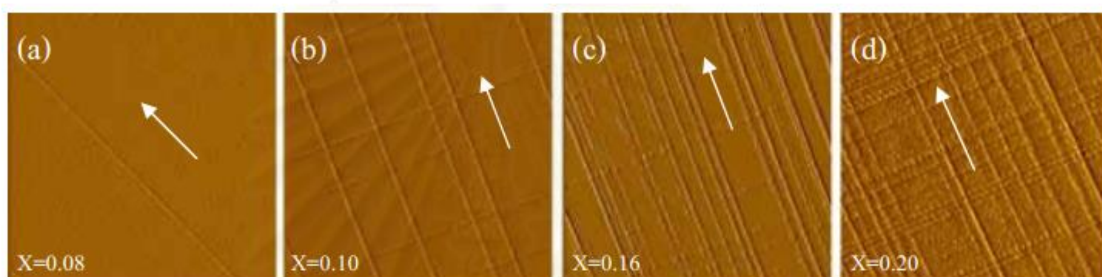

Figure 4.2 AFM images of InAs QDs on 50 nm InGaAs CHPs, where the molar fraction is (a) 0.08, (b) 0.10, (c) 0.16, and (d) 0.20, respectively [34].

In figure 4.2 demonstrates the AFM images of InAs QDs on InGaAs CHPs, where the thickness of all CHPs is 50 nm and *x* = 0.08, 0.10, 0.16 and 0.20, respectively. Figure 4.2(a) shows the AFM image of sample with *x* = 0.08, the dislocation only appears on [1-10] direction, called stripes. The QDs are aligned along the stripe in the form of chain, which is called quantum dot chain. Figure 4.2(b)-(d)

demonstrated complete CHPs on both [1-10] and [110] directions with QDs grew on top. It is clear that with higher value of *x*, the density of CHPs become higher.

4.1.2 The Effects of InGaAs Thickness, *y*

Aside from the effects of the molar fraction, the thickness of InGaAs layer also has effect on the accumulative strain and the surface of CHPs. When the thickness of InGaAs layer exceeds the H_c, the strain in InGaAs is decreased rapidly. Figure 4.3 shows AFM images for various thickness of $In_{0.15}Ga_{0.85}As$ CHPs. Figure 4.3(b) and 4.3(c) demonstrate the ineffective ordering of QDs relative to the thickness of CHPs layer.

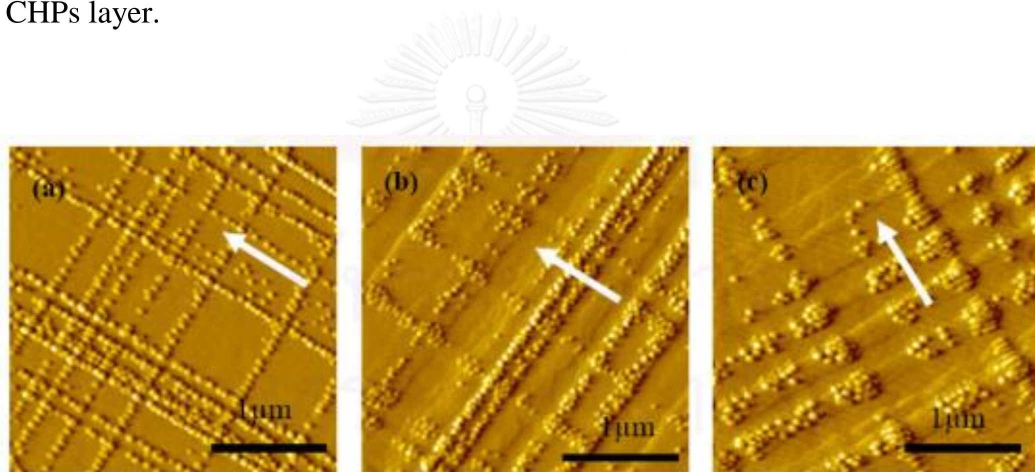

Figure 4.3 AFM images of InAs QDs on $In_{0.15}Ga_{0.85}As$ with the thickness of (a) 50 nm, (b) 100 nm, and (c) 150 nm, respectively. The arrow is pointing to [1-10] direction [35].

4.1.3 The Effects of Growth Interruption Time

Another parameter that affects CHPs, other than the molar fraction of In and the thickness of InGaAs layer, is the growth interruption (GI) time. GI is a time after the shutter of In cell is closed until the next growth process. For InAs QDs on flat GaAs surface, the GI time for the best optical result and FWHM is 30 s [36]. Similarly for InAs QDs on CHPs, the GI time for best optical result is also 30 s [37]. In the case of short GI time, the QDs are be able to form on the flat surface, as shown in figure 4.4(a) with white arrows. The sample of GI time of 30 s shows the best result, as shown in figure 4.4(b). Figure 4.4(c) shows the case of long GI time, the QDs shape becomes abnormal due to the In evaporation from the surface.

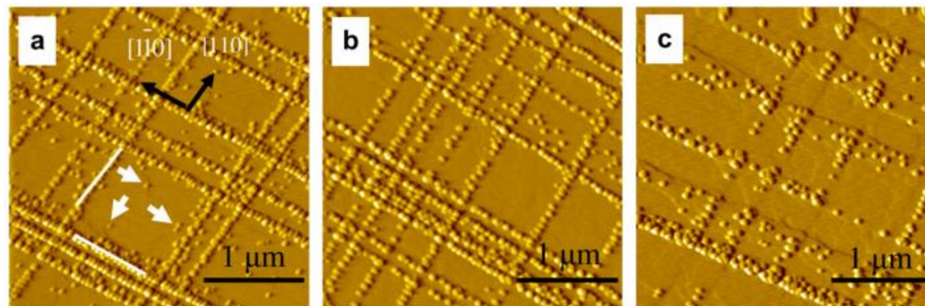

Figure 4.4 AFM images of InAs QDs on $In_{0.15}Ga_{0.85}As$ with GI time of (a) 0, (b) 30, and (c) 60 seconds [37].

4.1.4 Evolution of InAs Quantum Dots on Cross-Hatch Patterns, *z*

The height of InAs QDs on CHPs is different in each location, which indicated the difference in the formation time. The studied from T. Limwongse [28] shows the image threshold from AFM images of the QDs on CHPs sample with x = 0.2 and 50 nm thick. The evolution of InAs QDs formation on CHPs is concluded. The first location that QDs are formed was at the cross section of [1-10] and [110], as shown in figure 4.5(b). Followed by the formation along [1-10] direction, shown in figure 4.5(c). Then the QDs formed on [110] direction and the flat surface, respectively. The reason behind this evolution of QDs formation is due to difference in strain energy in each location.

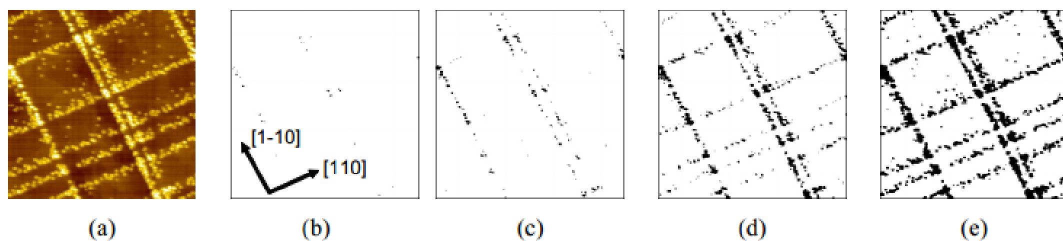

Figure 4.5 (a) AFM image of InAs QDs on $In_{0.2}Ga_{0.8}As$ CHPs with height contrast of 7.6 nm. And the images threshold with height contrast of (b) 5.5, (c) 4.9, (d) 4.0, and (e) 3.0 nm, respectively. The black color indicates the higher area and the white color indicates the lower area [34].

4.2 Subcritical Thickness Structures

Subcritical thickness or intermediate stage is a structure that forms when the thickness of epitaxial layer is below the h_c. In the cases of InAs on GaAs, this stage is in the range of 1.0-1.6 ML [12, 13]. The formation of nanostructures in the subcritical range is still poorly understood. According to figure 2.4, the subcritical thickness for InAs on GaAs falls into FM growth mode, because the lattice mismatch between them is approximately 0.072. The FM growth mode is considered as 2D growth mode. However, due to the potential energy during the growth could make the WL to be in a metastable state and could form 3D structures.

4.2.1 Quantum Dots Formation in Subcritical Thickness

Although the epitaxial layer of subcritical thickness is in 2D growth mode, the kinetic energy during the growth could make the WL to be in a metastable state and form into 3D structures. The studied by Tonkikh et al. [31] presented the transmission electron microscopy (TEM) image of InAs QDs formation on GaAs substrate, where InAs layer thickness is at 1.4 ML, as shown in figure 4.6. This experiment proved that the formation of QDs is possible even at subcritical thickness layer.

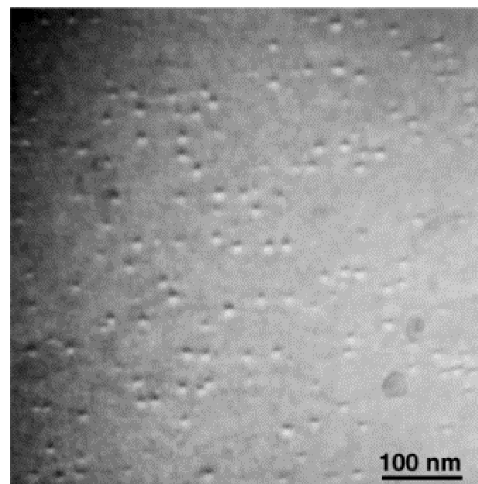

Figure 4.6 TEM image of subcritical thickness InAs QDs at 1.4 ML grown on GaAs substrate [31].

Moreover, the studied by V.G. Dubrovskii et al. [38] presented the density of InAs QDs grown on 5° off-cut GaAs(100) substrate with the thickness between 1.3,

1.4, and 1.5 ML. By looking at their PL spectra, the surface density can be obtained. Figure 4.7 clearly shown PL images of the density of InAs QDs, which indicated that when the thickness of epitaxial layer increases, the density of QDs is also increases. This proved that the ultra-low density of QDs can be obtained by the growth of subcritical thickness structure.

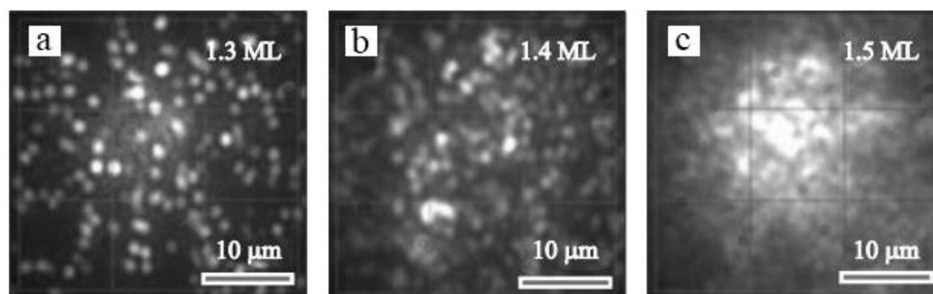

Figure 4.7 PL images of the density of (a) 1.3, (b) 1.4, and (c) 1.5 ML of InAs QDs grown on GaAs substrates [38].

4.2.2 Complex Structure in Subcritical Thickness

Other studied on subcritical thickness InAs layer showed an interesting structure that formed into wires and complex parquet structure as performed by Guryanov et al. [12]. The InAs layers of 1.0-1.5 ML were deposited on GaAs(100) singular and vicinal surfaces. The growth temperature is 470°C for InAs deposition. After the growth of InAs layer, the temperature is decreased down to 300°C for transferring to scanning tunneling microscopy (STM) operation.

The STM images of 1.0 and 1.5 ML of InAs on singular samples are shown in figure 4.8(a)-(c). In figure 4.8(a), the thickness of InAs is 1.0 ML with growth interrupt (GI) of 30 seconds, the image showed sign of wires along [001] direction. The lateral size of wires is approximately 30 nm. In figure 4.8(b) and (c), the thickness of InAs is 1.5 ML with GI of 30 and 2 seconds respectively, the images showed a so-called “parquet” structure, which resulted in perpendicular direction: [001] and [010]. In addition, a parquet model is depicted in figure 4.8(d) as clarification.

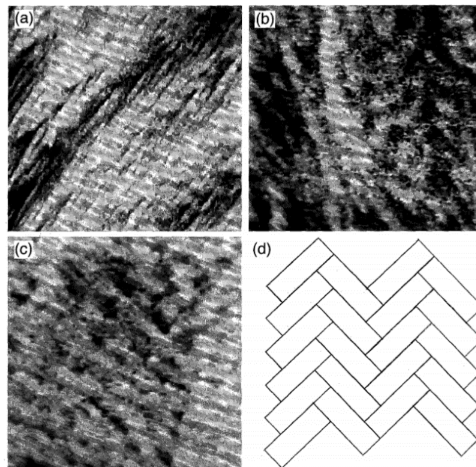

Figure 4.8 STM images of (a) InAs 1 ML with 30s GI, (b) InAs 1.5 ML with 30s GI, and (c) InAs 1.5 ML with 2s GI on singular GaAs(100) substrate. (d) A model of simple parquet structure for clarification [12].

On the other hand, the surface arrangements for vicinal samples are different than those on the singular samples. Figure 4.9(a) demonstrates the structure of the 1.0 ML InAs layer with GI of 30 seconds, the STM image shows similar result as found in singular sample, which revealed wires structure along [001] direction with a tilted angle by 15°. The lateral size of the wires is about 25 nm. Where in figure 4.9(b), InAs layer of 1.5 ML thick with GI of 2 seconds shows wires along the [001] direction but accompanied by wires with larger width that tilted slight toward [011] direction.

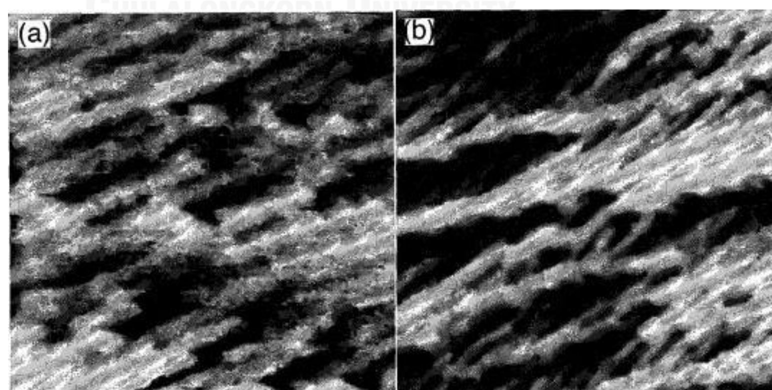

Figure 4.9 STM images of (a) InAs 1 ML with 30s GI and (b) InAs 1.5 ML with 2s GI on vicinal GaAs(100) substrate [12].

4.2.3 Horizontal Nanowires in Subcritical Thickness

Recently, the rather simple growth process of subcritical thickness of Ge on Si have been studied by Zhang et al. [11] who show horizontal nanowires (HNWs) of Ge/Si formed by submonolayers deposition and post annealing. The 3D islands called, “hut-clusters”, formed during annealing period. AFM images of this experiment are shown in figure 2.8. In this studied, the amount of deposited Ge on Si is 4.4 ML, which is 0.1 ML lower than h_c. After the deposition of Ge, the experiment was carried on by *in situ* annealing at 10°C lower than the growth temperature for 1 hour, 3 hours, and 12 hours. The annealing period affects in length of the HNWs.

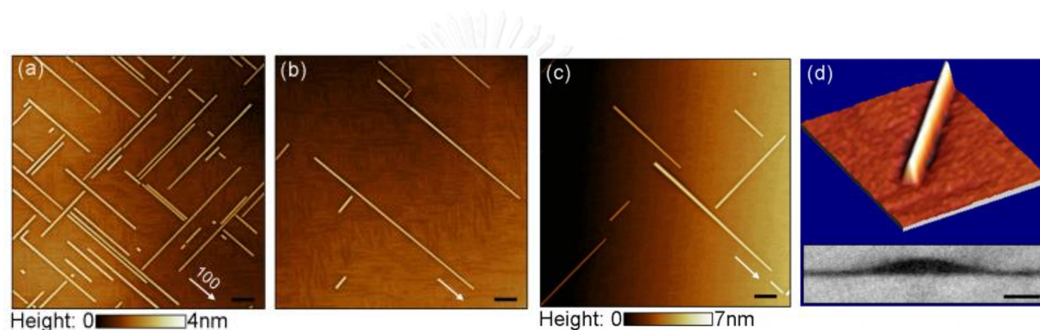

Figure 4.10 AFM images of Ge HNWs on Si substrates with (a) high and (b) low density of Ge HNWs. (c) Ge HNWs with miscut angle. (d) 3D AFM image with cross-sectional image indicated in the inset [11].

Figure 4.10(a) and 4.10(b) show the high and low density of Ge HNWs after *in situ* annealing for 12 hours. The HNWs direction are along [001] and [010] direction. The tapered Ge HNWs with a miscut angle are shown in figure 4.10(c). The 3D AFM image in figure 4.10(d) indicated that the HNWs are in the triangular shape with an image of cross-sectional shown in the inset.

4.3 Surface Morphology of Subcritical Thickness InAs on Cross-Hatch Patterns

All of the structures are grown on epi-ready GaAs (001) substrate. After the surface oxide removal at 580°C, GaAs buffer layer with the thickness of 300 nm is grown on top at the same temperature. A 25-nm $In_{0.2}Ga_{0.8}As$ CHP is grown on top of the flattened surface at 500°C, with the growth rate of 0.2 and 0.05 ML/s for Ga and In, respectively. The followed by growth interruption (GI) for 20 seconds before growing 6nm of GaAs spacer layer and GI for another 20 seconds. Finally, the

subcritical thickness of InAs layer with the growth rate of 0.02 ML/s is grown on top of GaAs spacer layer for 1.6, 1.5, and 1.4 ML. There are 2 groups of samples; annealed and non-annealed samples. In the case of annealed samples, the samples were left exposed with As_4 flux for 4 minutes and 30 seconds and the temperature of the sample is lowered to 470°C. The cross-sectional structures of the samples are shown in figure 4.11.

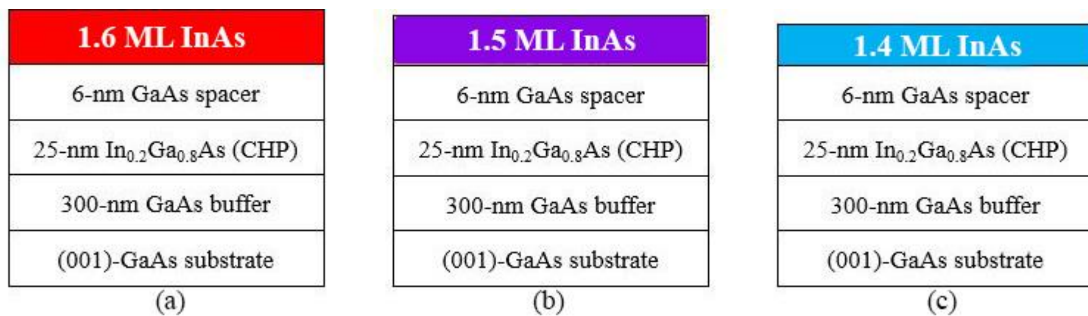

Figure 4.11 Cross-sectional structures of (a) 1.6 ML, (b) 1.5 ML, and (c) 1.4 ML subcritical InAs layer on $In_{0.2}Ga_{0.8}As$ CHPs.

The samples are separated into 2 groups: annealed and non-annealed samples. Each group contains 3 samples with varied thickness of InAs layer, which equal to 6 samples in total. This way the effect of thickness and the effect of annealing can be observed. For clarification, the overall samples and procedures are shown in table 2 below.

จุฬาลงกรณ์มหาวิทยาลัย
Chulalongkorn University

Table 2 Overall procedures for each sample

No.	Sample	Code	Thickness (ML)	Annealing Time (min)	Annealing Temp. (°C)
1	A_16	151014_A	1.6	4:30 min	470°C
2	A_15	151014_B	1.5	4:30 min	470°C
3	A_14	151021	1.4	4:30 min	470°C
4	NA_16	151118_A	1.6	0	N/A
5	NA_15	151029_B	1.5	0	N/A
6	NA_14	151118_B	1.4	0	N/A

4.3.1 Surface Morphology of Annealed Samples

This set of experiment contains sample A_16, A_15, and A_14. Each sample has the same growth structure but differed in the thickness of InAs layer. During the experiment, the pressure is kept at $1x10^{-7}$ Torr by continuously feeding As_4 flux. The *in situ* real time observation is done by 15kV RHEED. During the growth of InAs layer, RHEED patterns showed no sign of spotty patterns, which indicated that there are no 2D to 3D transition. After the subcritical thickness InAs growth process is finished, all 3 samples were left to annealed at 470°C for 4 minutes and 30 seconds under As_4 flux, the RHEED patterns after annealing period for sample A_16, A_15, and A_14, are shown in figure 4.12(a)-(c), respectively.

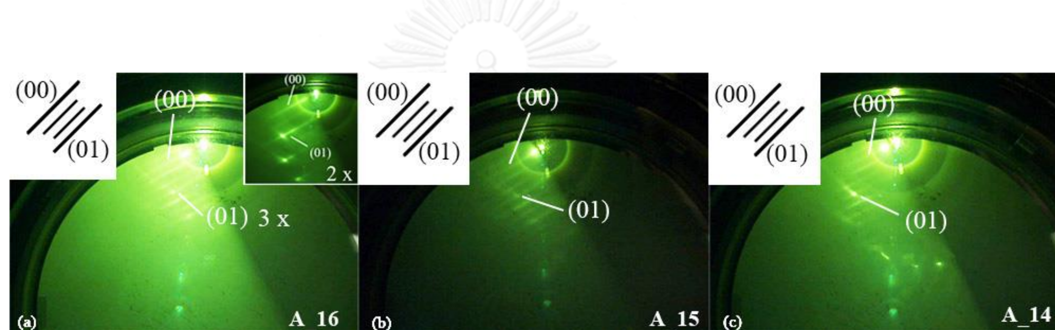

Figure 4.12 RHEED patterns for sample (a) A_16 with the inset showing (2 x *) surface reconstruction, (b) A_15, and (c) A_14 after the annealing process.

The RHEED results from all 3 samples appeared to have a similar pattern. The patterns show a (2 x 3) surface reconstruction, which is differed from flat surface, which has a (2 x 4) surface reconstruction [39]. When the electron beam hit the surface along [110] direction, the pattern appeared to be (2 x *) surface reconstruction, as shown in the inset of figure 4.12(a). On the other hand, when the electron beam hit the surface along [1-10] direction, the pattern appeared to be (* x 3) surface reconstruction. The (2 x 3) for subcritical thickness structure is in agreement with the studied by K. H. Ploog et al [40], which stated that the (2 x 3) surface reconstruction appeared when the InAs layer is lower than the h_c.

After finished with the growth process with MBE machine, the samples were taken out for surface characterization with AFM. The AFM images for A_16, A_15, and A_14 are shown in figure 4.13(a)-(f). The scale for top rows is $5x5\mu m^2$ and the

scale for bottom rows is $2x2\mu m^2$, respectively. The perpendicular lines indicate the [110] and [1-10] crystalline directions.

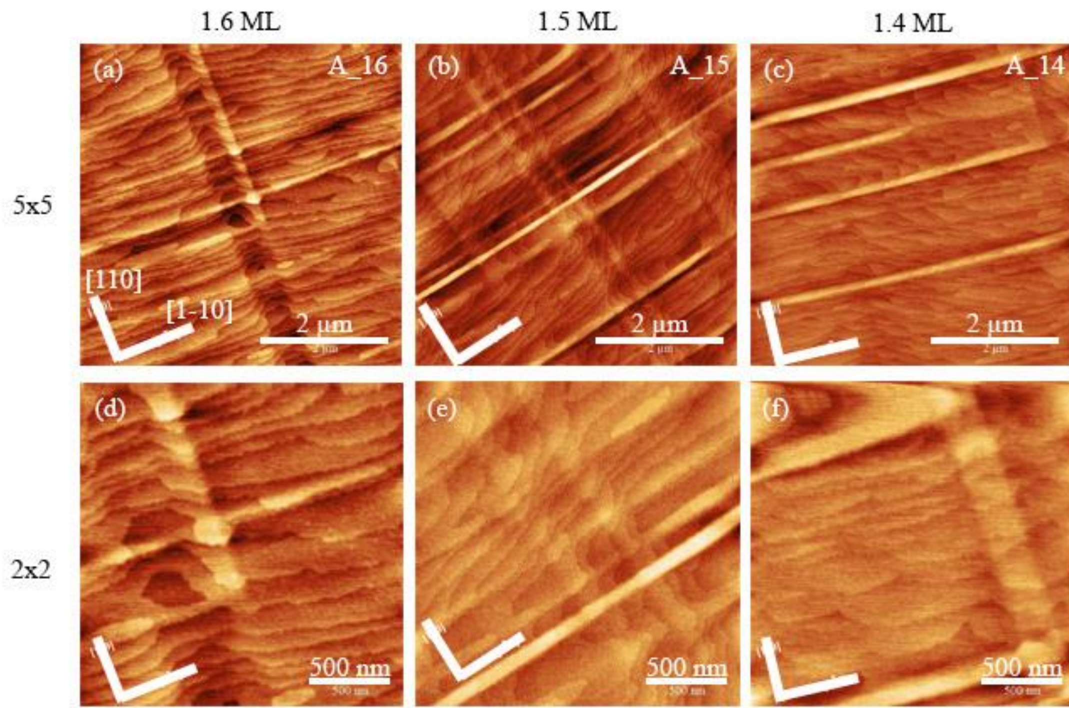

Figure 4.13 AFM images of (a)-(c) $5x5\mu m^2$ and (d)-(f) $2x2\mu m^2$ for sample A_16, A_15, and A_14, respectively.

According to the AFM images shown in figure 4.13, it can be clearly seen that the CHPs are formed along [110] and [1-10] direction as expected. However, the density of CHPs in each sample is different due to the dependent in growth environment, which caused by many factors: thermal conductivity from difference Mo Block, growth rate calibration, and the location of the sample when mounted onto the Mo Block.

Although the density of CHPs is different but the surface morphology shows some interesting nanostructures in all the samples. By comparing to the surface of the InAs QDs samples, the area that does not affect by the CHPs tends to be flat. However, the surface morphology of subcritical thickness InAs layer does not show any sign of flat surface, but seem to form into wire-like structures along [1-10] direction instead. This formation resembled to the report from Guryanov et al. [12], which reports that a similar wire-like structures. These wire-like formation are

possibly due to the applied external stress during the lattice mismatched growth system [41].

4.3.2 Surface Morphology of Non-Annealed Samples

To understand the annealing effect on subcritical thickness InAs layer on InGaAs CHPs, the samples with non-annealing period are also needed to be study. The growth process for non-annealed samples is the same as the annealed samples. But after the deposition of subcritical thickness InAs layer, the OM temperature was step down to 100°C immediately. By doing this, there will be no kinetic energy after the InAs deposition. The non-annealed samples are named NA_16, NA_15, and NA_14, which differed in thickness accordingly.

The real time surface reconstruction for non-annealed samples is also observed by *in situ* RHEED, as shown in figure 4.14 (a)-(c). Even though there were no annealing period, but the RHEED patterns after the subcritical thickness InAs layer for all 3 samples showed the same pattern as in annealed samples, which is also (2 x 3) surface reconstruction. This is also similar studied by Ploog et al [40], which explained that there are no difference in RHEED patterns with annealed and non-annealed samples at subcritical thickness, due to the absence of 3D islands.

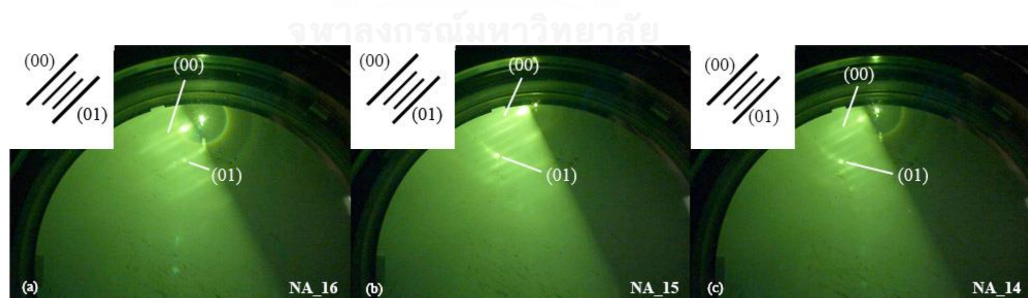

Figure 4.14 RHEED patterns for sample (a) NA_16, (b) NA_15, and (c) NA_14 after subcritical thickness InAs deposition.

When the growth process finished, all 3 samples then get taken out to carry on to analyzing the surface morphology by AFM. Figure 4.15(a)-(f) presents the AFM images of sample NA_16, NA_15, and NA_14, with indication of [110] and [1-10] crystalline direction. Where images on the top row displayed 5x5μm^2 and the bottom row displayed 2x2μm^2 scale.

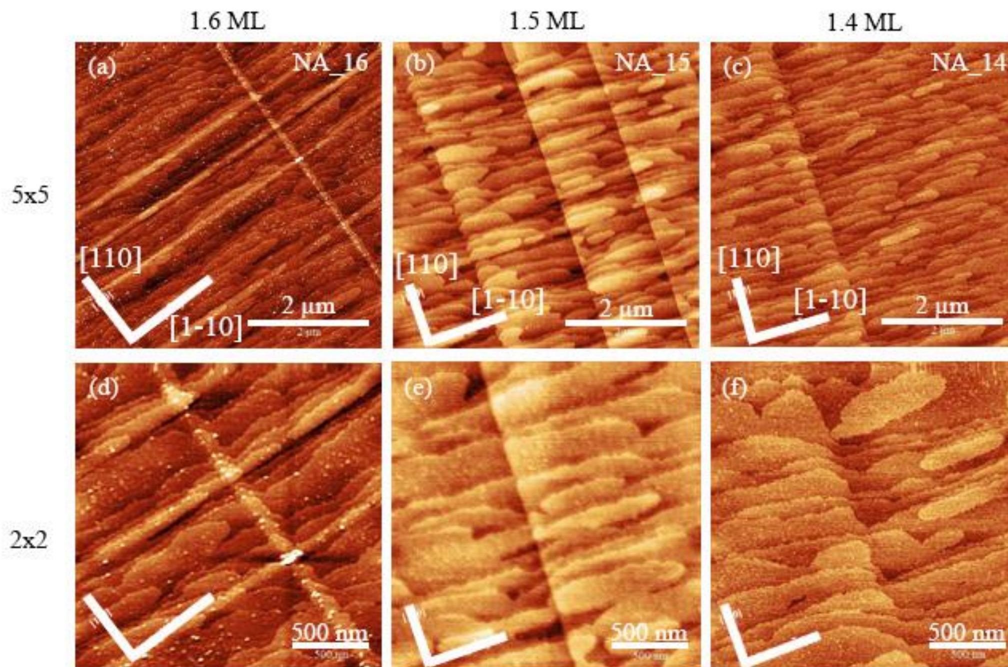

Figure 4.15 AFM images of (a)-(c) 5x5μm^2 and (d)-(f) 2x2μm^2 for sample NA_16, NA_15, and NA_14, respectively.

Although RHEED pattern for sample NA_16 did not show any spotty patterns, but after scanning the surface morphology by AFM, there are QDs formation on the surface, as shown in figure 4.15(a) and 4.15(d). However, it is considered as low density QDs when compared to the QDs formation at h_c [38]. There also exists a large QD in the middle of the CHPs, which is where the QDs tend to form first [8]. Aside from the QDs formation, it can be seen that there are also wire-like structure on the surface as well.

In the case of sample NA_15 and NA_14, there are no sign of QDs formation on the surface. However, the CHPs for both samples do not clearly show. As mentioned before, there are many factors that might affect the formation of CHPs. Even though the CHPs cannot be seen clearly, but the wire-like structure is also formed in these 2 samples, which is similar to sample NA_16, but without any QDs formation on the surface.

4.3.3 Effects of Thickness for Subcritical Thickness InAs Layer

The surface morphology for both annealed and non-annealed samples with subcritical thickness InAs layer on InGaAs CHPs were obtained by the AFM scanning system, which show interesting results. But to explain the difference between these samples, the effects of different thickness and *in situ* annealing of subcritical layer must be taken into account. Because, these 2 parameters are the main parameters that varied in each samples.

First, the surface topology for annealed samples has been analyzed to understand the effects of different thickness of subcritical thickness InAs layer. Figure 4.16(a)-(c) shows the surface morphology with its line scan on the side for annealed sample A_16, A_15, and A_14, respectively.

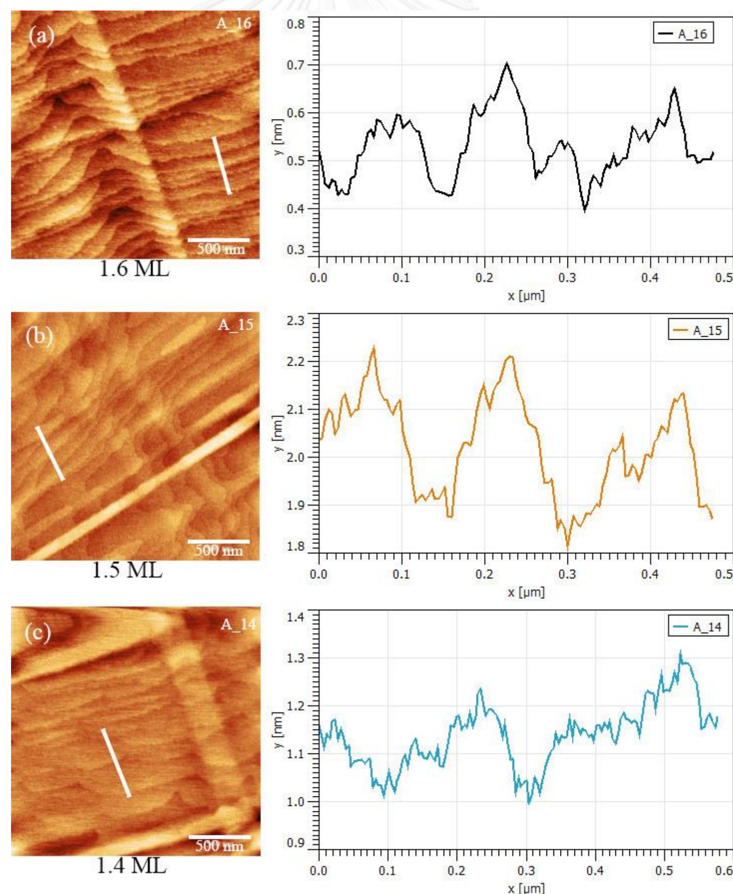

Figure 4.16 Surface morphology of 2x2μm^2 AFM images with line scan profiles of annealed sample (a) A_16, (b) A_15, and (c) A_14, respectively.

From the line scan profiles, there are noticeable trend of the distance between two peaks of atomic wires. For sample A_16, the distance between two peaks of the structure is approximately 100 nm. While the distance two peaks of sample A_15 is around 150 nm. And for sample A_14, the distance between peaks is around 200 nm. The reason for this effect can be explained by the strain relaxation of the lattice mismatch structure. When the value of InAs deposition layer is getting closer to that of h_c, in this case is 1.7 ML, there is more chances to perform a 2D to 3D transition, which mean that the 2D wetting layers are accumulating closer together before forming into 3D islands. That is why sample A_16, has a closer distance between peaks of atomic wires.

However, the height of atomic wire for each sample is range from 0.1 nm to 0.3 nm, where InAs thickness at 1.6 ML, 1.5 ML, and 1.4 ML, are equivalent to 0.485 nm, 0.454 nm, and 0.424 nm, respectively. Where, InAs with the thickness of 1 ML is equivalent to 0.3 nm. These mean that the varied thickness of subcritical thickness InAs layer does not affect the height of the atomic wire, but does affect the distance between peaks of the atomic wires instead. Since the height of the atomic wire is low, it can also be considered as a wetting layer, which falls between FM and SK_1 growth mode.

4.3.4 Effects of In Situ Annealing of Subcritical Thickness InAs Layer

The effects of varied thickness for subcritical thickness of InAs layer from 1.4 to 1.6 ML for annealed samples have been explained in the previous section. Now, the effects of *in situ* annealing of subcritical thickness InAs layer itself will be explain in this section, to see what happen when to the surface when it undergo *in situ* annealing.

For non-annealed samples, the surface topology is also has been analyzed by the same method. Figure 4.17(a)-(c) shows the surface morphology with its line scan on the side for non-annealed sample NA_16, NA_15, and NA_14, respectively.

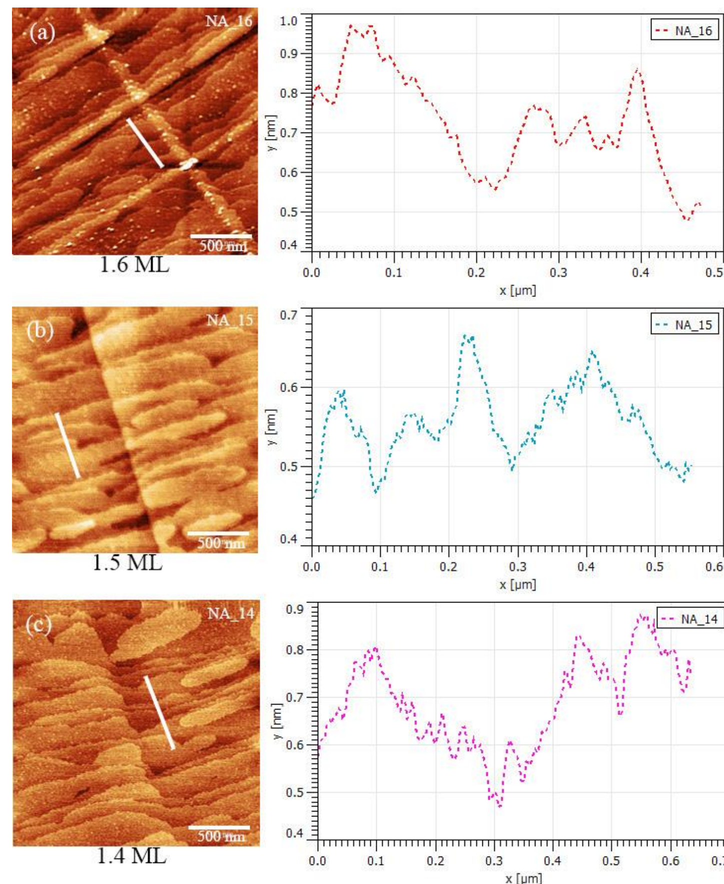

Figure 4.17 Surface morphology of 2x2μm^2 AFM images with line scan profiles of non-annealed sample (a) NA_16, (b) NA_15, and (c) NA_14, respectively.

From the line scan profile, the trends are similar with the annealed samples. However, the distance between atomic wires is different. In the case of sample NA_16, the distance between peaks of atomic wires is approximately 200 nm, as shown in figure 4.17(a). The distance is around 100 nm wider when compared to the annealed sample at the same thickness. Figure 4.17(b) shows the line scan profile for sample NA_15. The distance between two atomic wires is around 220 nm. Finally, figure 4.17(c) presents the line profile for sample NA_14, where the distance between two atomic wires becomes wider at around 300 nm.

For clarification of the effects of *in situ* annealing of subcritical thickness InAs, the mean wire separation for annealed and non-annealed are plotted in figure 4.18 below. Figure 4.18 illustrates the minimum and maximum values of the periodicity of atomic wires for all the samples.

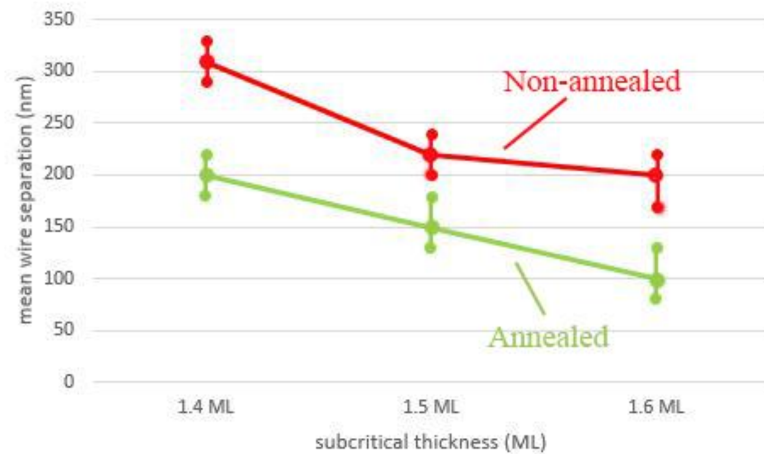

Figure 4.18 Mean wire separation data with minimum and maximum values of both non-annealed (red) and annealed (green) samples with subcritical thickness InAs layer of 1.4, 1.5, and 1.6 ML, respectively.

4.3.5 Effects of Cross-Hatch Patterns on Subcritical Thickness InAs Layer

Typically, when InAs QDs are formed on CHPs, they are initially formed at the intersection point first, followed by [1-10] and then [110] direction [34]. Although the experiments in this thesis is a subcritical thickness InAs layer on InGaAs CHPs, but it showed the same effects as InAs QDs on CHPs. Figure 4.19(a) shows great example of 5x5μm^2 AFM image of sample A_14, which contains both formation of subcritical thickness InAs layer on the intersection and along [1-10] direction. The line scans in figure 4.19(b) are done along [110] and [1-10] direction to observe the confinement and elongation of both directions.

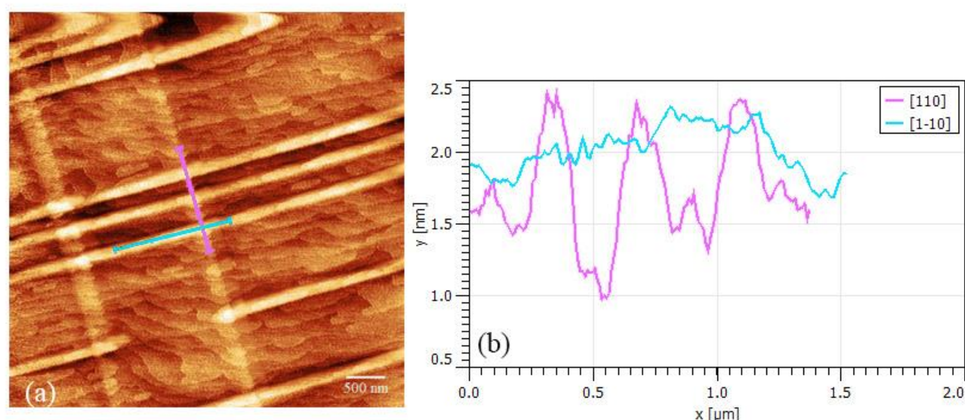

Figure 4.19 (a) 5x5μm^2 AFM image of sample A_14 with (b) line scan profiles along [110] (pink) and [1-10] (blue) directions.

As shown in figure 4.19, the height of the structure along [110] direction becomes discrete on CHPs. On the other hand, the structure along [1-10] direction is shown as a continuous structure. The highest peak is of course at the intersection of CHPs. But along [1-10] direction on CHPs, the subcritical thickness InAs layer is formed into a wire on CHPs. The potential application of this kind of structure could be uses in many types of semiconductor devices, such as MOSFET.

4.3.6 Effects of Long-Time Annealing on Subcritical Thickness InAs Layer

Apart from the effects of short-time annealing experiment on subcritical thickness InAs layer on InGaAs CHPs, the effects of long-time annealing were also observed. The structure of the samples that were used in this experiment have the same exact same structure as the previous experiment with the thickness of InAs at 1.6 ML. However, the annealing time is a lot longer when compared the short-time annealing, at 1 and 2 hours [42].

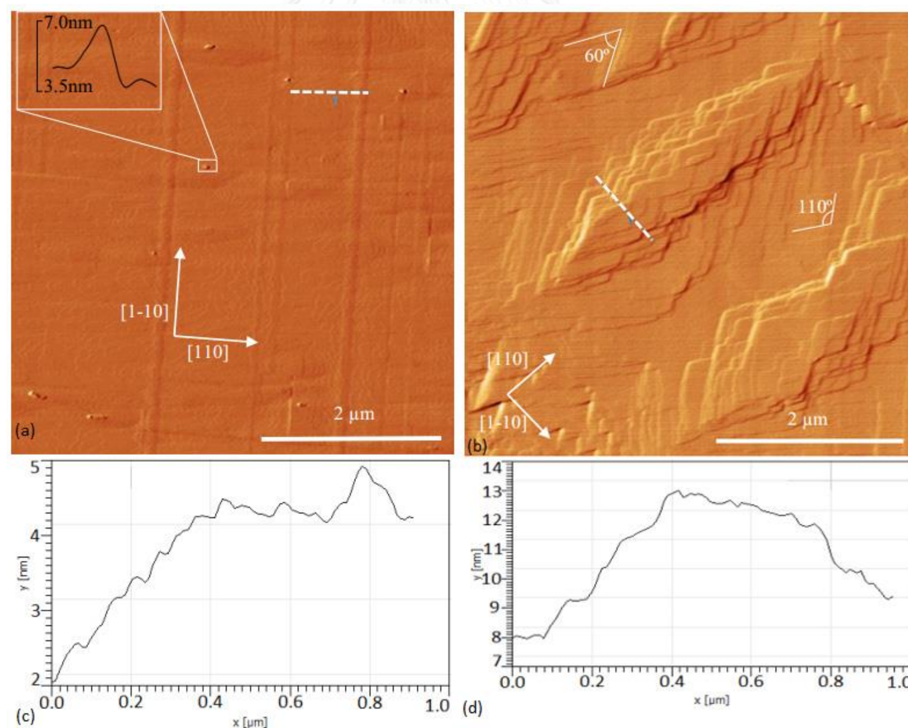

Figure 4.20 5x5µm^2 AFM images of (a) 1-hour-annealed with the inset of line scan of QDs and (b) 2-hour-annealed sample. Where (c) and (d) are line scan profiles for (a) and (b), respectively [42].

The AFM images and line profiles of both samples are shown in figure 4.20. For 1-hour-annealed sample, the AFM image is shown in figure 4.20(a); the CHPs can be seen clearly with the dominant stripes along [1-10] direction. The inset in figure 4.20(a) shows the size of the QDs formed on the surface, which is around 3.5 nm high with the line scan profile in figure 4.20(c) Moreover, the more interesting structure occurred from 2-hour-annealed sample, where the surface becomes hill-like structure, as shown in figure 4.20(b). For 2-hour-annealed sample, the CHPs are completely covered by the hill-like structure. The line scan profile of this structure in figure 4.20(d) shows the thickness of the structure, where it is clear that it is in the form of steps. Each step is approximately 1 nm. The presumption about the occurrence of this kind of structure is believed to be the digging effect of the GaAs spacer layer during the long-time annealing process.

4.4 Optical Properties of Subcritical Thickness InAs on Cross-Hatch Patterns

The optical properties of nanostructure are also one of the important factors for optoelectronic devices. This property determined the suitable application for different structure, which can be used in many kinds of applications. However, there are not many investigation have been done on the subcritical thickness InAs layer before.

จุฬาลงกรณ์มหาวิทยาลัย
Chulalongkorn University

4.4.1 Optical Properties of InAs QDs on Cross-Hatch Patterns

In general, optical properties of InAs QDs on InGaAs CHPs obtained by photoluminescence (PL) technique are usually depend on the size of QDs on both CHPs and flat surface. The experiment done by A. Jittrong [43] shows a result of PL spectrum of InAs QDs on $In_{0.2}Ga_{0.8}As$ CHPs with 6 nm of GaAs spacer, which is similar to this experiment. In figure 4.21 shows an AFM image of 1 stack sample and the corresponding PL spectrum measured at 20 K.

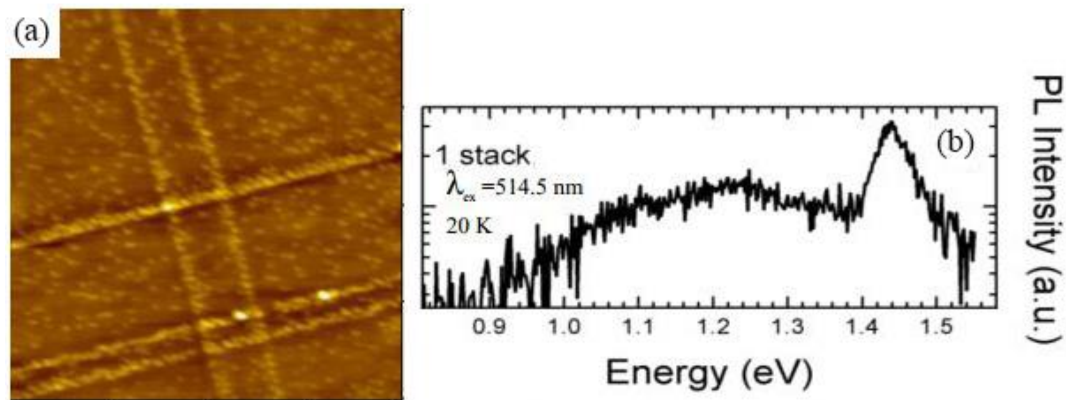

Figure 4.21 (a) 2x2μm^2 AFM image of InAs QDs on $In_{0.2}Ga_{0.8}As$ CHPs with 6 nm of GaAs spacer and (b) the corresponding PL spectrum [43].

The QDs formation showed in figure 4.21(a) shows that the QDs are formed on both CHPs and flat surface with large variety in size. The PL spectrum shows that due to the large variety in size and the area of formation of QDs caused the PL spectrum to be broader with a peak at 1.24 eV. At the same time, the WL and GaAs layer combined with carbon, emitted PL energy at 1.44 eV. However, there are no emission from InGaAs CHPs layer because of the thin GaAs spacer layer, which caused the tunneling effect of the carrier to go to the WL and QDs layer, resulted in reduction of emission from CHPs layer.

4.4.2 Optical Properties of Annealed Subcritical Thickness InAs on Cross-Hatch Patterns

Typically, the PL measurement was done with the GaAs capping layer to create a quantum well structure. However, the studied from M. J. Milla et al. [44] shows that the PL spectrum for InGaAs surface QDs can also be measured without the need of capping layer.

In this thesis experiment, the PL measurement for subcritical thickness InAs layer was done without the 100 nm GaAs capping layer. Also the sample that was choosing to measure was sample A_15, which displayed highest density of CHPs. The sample measured by the power dependent method, which varied the power of the laser to see the change in optical properties. Figure 4.22 shows the results of PL measurement of sample A_15 without GaAs capping layer.

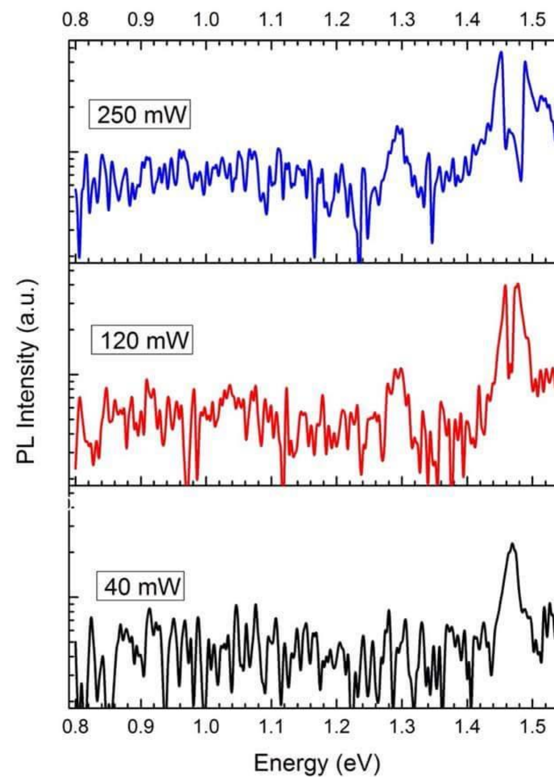

Figure 4.22 The power dependent PL spectrum of sample A_15 without GaAs capping layer.

From figure 4.22, the power of the laser was varied from 40 mW, 120 mW, to 250 mW. The PL peak at 1.24 eV, which correspond to InAs QDs, cannot be found since there is no QDs formation. However, there are a peak at 1.29-1.30 eV, which is assume to be InGaAs CHPs [45]. Moreover, the peaks for InAs atomic wires and GaAs layer are separated from each other at 1.45 eV and 1.49 eV, respectively. Although the intensity of the PL energy is low, but this PL measurement proves that even without GaAs capping layer, the surface structure still emit photons indicating that it may be useful in optoelectronics applications.

Chapter 5

Conclusions

This thesis reports the studies of the surface morphology and topology of subcritical thickness InAs nanostructures on $In_{0.2}Ga_{0.8}As$ CHPs, grown by molecular beam epitaxy.

The samples were separated into 2 groups differentiated by the post-growth process: annealed and non-annealed samples. The real time RHEED observation did not show any sign of 3D islands formation for both groups of samples, which indicated that the thickness is lower than h_c. However, it does not mean that there was no 3D islands formation, since it has been found in non-annealed sample with 1.6 ML of InAs layer, even though they are low density QDs.

The surface morphologies for both annealed and non-annealed samples displayed similarity in the terms of structural. The surface of both groups appear to formed into wire-like structures, with a mean height of 0.3 nm, which is equivalent to 1 ML of InAs layer. However, the different between annealed and non-annealed subcritical thickness InAs nanostructures can be distinguished by the distance between two atomic wires. In case of annealed samples, the distance between atomic wires seems to be narrower than the non-annealed samples. This effect is believed to cause by the kinetic energy during the annealing period.

$In_{0.2}Ga_{0.8}As$ CHPs also has effect on the formation of subcritical thickness InAs layer as well. The evolution of subcritical thickness InAs on CHPs agrees with the evolution of InAs QDs, where the first position to form is at the intersection of CHPs. However, the formation of subcritical thickness on CHPs is confined on [110] direction and elongated along [1-10] direction, which InAs tends to favor.

The optical properties of uncapped subcritical thickness InAs on CHPs shows that it is possible to do PL measurement without GaAs capping layer. The PL peak gives the highest energy at 1.45 eV, which is a peak of InAs atomic wires. These conclude that there is no 3D islands transformation on the surface after annealing period.

This thesis experiments are done to understand the formation of subcritical thickness InAs layer on InGaAs CHPs. At the subcritical or intermediate stage, there are still a lot to be discover. The results from this thesis could be useful for further studies in the subcritical region not only InAs structure, but other structure as well.

REFERENCES

1. Liu, Z., et al., *High-detectivity InAs nanowire photodetectors with spectral response from ultraviolet to near-infrared.* Nano Research, 2013. **6**(11): p. 775-783.
2. Coleman, J.J., J.D. Young, and A. Garg, *Semiconductor quantum dot lasers: a tutorial.* Journal of Lightwave Technology, 2011. **29**(4): p. 499-510.
3. Chuang, S., et al., *Ballistic InAs nanowire transistors.* Nano Lett, 2013. **13**(2): p. 555-8.
4. Chakrabarti, S., et al., *Spin-polarized light-emitting diodes with Mn-doped InAs quantum dot nanomagnets as a spin aligner.* Nano Lett, 2005. **5**(2): p. 209-12.
5. Park, M.H., et al., *Effect of growth temperature and quantum structure on InAs/GaAs quantum dot solar cell.* J Nanosci Nanotechnol, 2014. **14**(4): p. 2955-9.
6. Wang, H., et al., *A top-down approach to fabrication of high quality vertical heterostructure nanowire arrays.* Nano Lett, 2011. **11**(4): p. 1646-50.
7. Ovid'ko, I. and A.G. Sheinerman, *Enhanced formation of nanowires and quantum dots on dislocated substrates.* Journal of Physics, 2004. **16**: p. 2161-2170.
8. Kanjanachuchai, S. and T. Limwongse, *Nucleation sequence of InAs quantum dots on cross-hatch patterns.* J Nanosci Nanotechnol, 2011. **11**(12): p. 10787-91.
9. Himwas, C., S. Panyakeow, and S. Kanjanachuchai, *Optical properties of as-grown and annealed InAs quantum dots on InGaAs cross-hatch patterns.* Nanoscale Res Lett, 2011. **6**(1): p. 496.
10. Kanjanachuchai, S., et al., *Self-assembled InAs quantum dots on cross-hatch InGaAs templates: Excess growth, growth rate, capping and preferential alignment.* Microelectronic Engineering, 2009. **86**: p. 844-9.
11. Zhang, J.J., et al., *Monolithic growth of ultrathin Ge nanowires on Si(001).* Phys Rev Lett, 2012. **109**(8): p. 085502.

12. Guryanov, G.M., et al., *An intermediate (1.0-1.5 monolayers) stage of heteroepitaxial growth of InAs on GaAs(100) during submonolayer molecular beam epitaxy.* Surface Science, 1996. **352**(354): p. 646-650.
13. Tonkikh, A.A., et al., *Quantum Dots in InAs Layers of Subcritical Thickness on GaAs(100).* Technical Physics Letters, 2003. **29**(8): p. 691-693.
14. Sugawara, M., *Theoretical based of the optical properties of semiconductor quantum nano-structures.* Semiconductors and Semimetals: Self-assembled InGaAs/GaAs quantum dots, 1999: p. 1-116.
15. Bhattacharya, P., *Properties of Lattice-matched and Strained Indium Gallium Arsenide*. 1993: INSPEC, the Institution of Electrical Engineers.
16. Haapamaki, C.M. and R.R. Lapierre, *Mechanisms of molecular beam epitaxy growth in InAs/InP nanowire heterostructures.* Nanotechnology, 2011. **22**(33): p. 335602.
17. Rieger, T., D. Grutzmacher, and M.I. Lepsa, *Misfit dislocation free InAs/GaSb core-shell nanowires grown by molecular beam epitaxy.* Nanoscale, 2015. **7**(1): p. 356-64.
18. Lieten;, R.R., et al., *Growth of InN on Ge(1 1 1) by molecular beam epitaxy using GaN buffer.* Journal of Crystal Growth, 2008. **310**(6): p. 1132-1336.
19. Simmons, J.H. and K.S. Potter, *Optical Materials*. 2000: Academic Press.
20. Adachi, S., *Physical Properties of III-V Semiconductor Compounds*. 1992: Wiley.
21. Daruka, I. and A.L. Barabasi, *Dislocation free island formation in heteroepitaxial growthL A study at equilibrium.* Physical Review Letters, 1997. **79**: p. 3708-3811.
22. Bimberg, D., M. Grundmann, and N.N. Ledentsov, *Quantum Dot Heterostructure*. 1998, Chichester: Wiley.
23. Adolfsson, G., et al., *High-performance long-wavelength InGaAs/GaAs multiple quantum-well lasers grown by molecular beam epitaxy.* IEEE Journal of Electronics, 2007. **43**(8): p. 454-456.
24. Andrews, A.M., et al., *Modeling cross-hatch surface morphology in growing mismatched layers.* Journal of Applied Physics, 2002. **91**(4): p. 1933-1943.

CHULALONGKORN UNIVERSITY

25. Tamura, M., A. Hashimoto, and Y. Nakatsugawa, *Threading dislocations in InxGa1-xAs/GaAs heterostructures.* Journal of Applied Physics, 1992. **72**(8): p. 3398-3405.
26. Ramanov, A.E., et al., *Threading dislocation reduction in strained layers.* Journal of Applied Physics, 1999. **85**(1): p. 3398-3405.
27. Matthews, J.W. and A.E. Blanklsee, *Defects in epitaxial multilayers *: I. Misfif dislocations.* Journal of Crystal Growth, 1974. **27**.
28. Limwongse, T., S. Panyakeow, and S. Kanjanachuchai, *Evolution of InAs quantum dots grown on cross-hatch substrates.* Physica Status Solidi C, 2009. **6**(4): p. 806-809.
29. Himwas, C., *Growth and Characterization of Stacked InAs Quantum Dots on Cross-Hatch Patterns*, in *Electrical Engineering*. 2011, Chulalongkorn University: Faculty of Engineering.
30. Thet, C.C., *Growth and Characterization of Ordered InAs Quantum Dots on Cross-Hatch Virtual Substrate*, in *Electrical Engineering*. 2006, Chulalongkorn University: Faculty of Engineering.
31. Tonkikh, A.A., et al., *Formation of Semiconductor Quantum Dots in The Subcritical Thickness Range.* International Journal of Nanoscience, 2007. **6**(5): p. 339-343.
32. Cui, Y., et al., *Nanowire nanosensors for highly sensitive and selective detection of biological and chemical species.* Science, 2001. **293**(5533): p. 1289-92.
33. Li, L.H., et al., *Growth-interruption-induced low-density InAs quantum dots on GaAs.* Journal of Applied Physics, 2008. **104**(083508): p. 4.
34. Limwongse, T., *Evolution of InAs Quantum Dots Grown on Cross-Hatch Substrates*, in *Department of Electrical Engineering Faculty of Engineering*. 2008, Chulalongkorn University.
35. Thet, C.C., et al., *The Effect of Relaxed InGaAs Virtual Substrates on the Formation of Self-Assembled InAs Quantum Dots.* Semiconductor Science and Technology, 2008. **23**(055007).

36. Kiravittaya, S., *Homogeneity improvement of InAs/GaAs self-assembled quantum dots grown by molecular beam epitaxy*, in *Department of Electrical Engineering Faculty of Engineering*. 2002, Chulalongkorn University.
37. Thet, C.C., S. Panyakeow, and S. kanjanachuchai, *Growth of InAs quantum-dot hatches on InGaAs/GaAs cross-hatch virtual substrates.* Microelectronic Engineering, 2007. **84**(5-8): p. 1562-1565.
38. Dubrovskii, V.G., et al., *Ultra-low density InAs quantum dots.* Semiconductors, 2013. **47**(10): p. 1324-1327.
39. Kiravittaya, S., et al. *In-situ RHEED investigation of MBE-grown InAs QDs on (0 0 1) GaAs epilayer*. in *Electrical Engineering Conference*. 2000.
40. K.H. Ploog and O. Brandt, *InAs monolayers and quantum dots in a crystalline GaAs matrix.* Semiconductor Science and Technology, 1993. **8**(1S): p. S229.
41. Guinier, A., R. Jullien, and I.U.o. Crystallography, *The solid state: from superconductors to superalloys*. 1989: International Union of Crystallography.
42. Eiwwongcharoen, W., et al. *The Effects of Long-Time Annealing of Subcritical InAs Layer on Cross-Hatch Patterns*. in *EECON 37*. 2014.
43. Jittrong, A., *The Effects of Reduced Spacer Thickness Towards Polarized Photoluminescence of Multi-Stack InAs Quantum Dots on Cross-Hatch Patterns*, in *Electrical Engineering*. 2014, Chulalongkorn University: Faculty of Engineering.
44. Milla, M.J., J.M. Ulloa, and A. Guzman, *High optical sensitivity to ambient conditions of uncapped InGaAs surface quantum dots.* Applied Physics Letters, 2012. **100**(131601): p. 3.
45. Chokamnuai, T., *Polarized Photoluminescence of Vertically Stacked InAs Quantum Dots on Cross-Hatch Patterns*, in *Electrical Engineering*. 2013, Chulalongkorn University: Electrical Engineering.

จุฬาลงกรณ์มหาวิทยาลัย
Chulalongkorn University

APPENDIX

จุฬาลงกรณ์มหาวิทยาลัย
Chulalongkorn University

VITA

Win Eiwwongcharoen was born in Bangkok, Thailand on October 17, 1990. He received the Bachelor of Engineering in Electrical Engineering from Thammasat University, Thailand in April 2013.

He entered the Graduate School of Chulalongkorn University in June 2013, as a Master Degree student in Semiconductor Research Devices Laboratory (SDRL), in the Department of Electrical Engineering, Faculty of Engineering.